

RESEARCH ARTICLE

Rydberg quantum computation with nuclear spins in two-electron neutral atoms

Xiao-Feng Shi

*School of Physics and Optoelectronic Engineering, Xidian University, Xi'an 710071, China**E-mail: shixiaofeng@xidian.edu.cn**Received December 25, 2020; accepted March 18, 2021*

Alkaline-earth-like (AEL) atoms with two valence electrons and a nonzero nuclear spin can be excited to Rydberg state for quantum computing. Typical AEL ground states possess no hyperfine splitting, but unfortunately a GHz-scale splitting seems necessary for Rydberg excitation. Though strong magnetic fields can induce a GHz-scale splitting, weak fields are desirable to avoid noise in experiments. Here, we provide two solutions to this outstanding challenge with realistic data of well-studied AEL isotopes. In the first theory, the two nuclear spin qubit states $|0\rangle$ and $|1\rangle$ are excited to Rydberg states $|r\rangle$ with detuning Δ and 0, respectively, where a MHz-scale detuning Δ arises from a weak magnetic field on the order of 1 G. With a proper ratio between Δ and Ω , the qubit state $|1\rangle$ can be fully excited to the Rydberg state while $|0\rangle$ remains there. In the second theory, we show that by choosing appropriate intermediate states a two-photon Rydberg excitation can proceed with only one nuclear spin qubit state. The second theory is applicable whatever the magnitude of the magnetic field is. These theories bring a versatile means for quantum computation by combining the broad applicability of Rydberg blockade and the incomparable advantages of nuclear-spin quantum memory in two-electron neutral atoms.

Keywords alkaline-earth atom, Rydberg state, quantum computation, neutral atom

1 Introduction

It is widely believed that quantum information processing can carry out fantastic tasks beyond the capability of classical technology [1, 2], although unfortunately a universal quantum computer has not yet been realized especially because of the fast dissipation on the timescale of each system useful for realizing a quantum information processor [3–7]. Recently, neutral atoms have been recognized as a new promising platform for large-scale quantum computing [8–13] because quantum entanglement based on the dipole blockade between neutral Rydberg atoms can be generated rapidly in a large qubit array [14–25]. However, models for reliable and practical quantum computing need entangling gates with a fidelity beyond, for example, 0.999 [26], while the best experimental fidelity of two-qubit entangling gates with alkali-metal atoms is below 0.98 [22, 23].

A new route toward neutral-atom quantum computation is by using atoms with two valence electrons and a

nonzero nuclear spin, i.e., some alkaline-earth-metal or lanthanide atoms, which we call alkaline-earth-like (AEL) atoms. Compared to alkali-metal atoms, well-studied AEL atoms such as strontium and ytterbium can be more easily cooled to very low temperatures [25, 27–30] or to the vibrational ground state [31], their nuclear spin states are insensitive to background magnetic noise and can be preserved in the process of cooling [32], and long-lived trapping of both the ground and Rydberg states is realizable [33]. These properties compare favorably to those of alkali-metal atoms concerning quantum control for entanglement generation. A recent Rydberg blockade experiment [25] with alkaline-earth-metal atoms reported a two-atom entanglement fidelity 99.5%, while the best number with alkali-metal atoms is 97.4% [20, 22]. However, the entanglement in Ref. [25] is between a Rydberg state and a metastable state $(5s5p)^3P_0$ of the nuclear-spin-free strontium-88. In principle, by Rydberg blockade one can entangle nuclear spin qubit states in the ground-state space, but its realization faces an outstanding challenge, namely, that there is no hyperfine splitting in the ground state of well-known AEL fermions like strontium-87 and ytterbium-171 and it is unlikely to leave one nuclear spin qubit state unaffected when rotating the other qubit state back and forth to Rydberg state with a megahertz rate.

In this work, two theories, Theory 1 and Theory 2, are

*arXiv: 2103.13847. Special Topic: Trapped Atoms and Ions for Quantum Science (Eds. Le Luo, Kenji Toyoda, Kihwan Kim, Jaewook Ahn & Dzmitry Matsukevich). This article can also be found at <http://journal.hep.com.cn/fop/EN/10.1007/s11467-021-1069-6>.



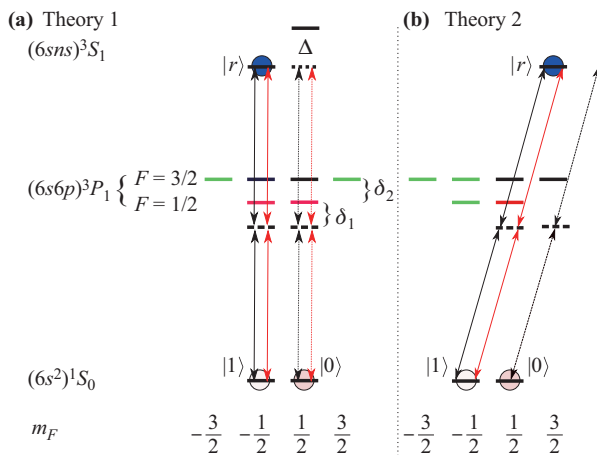


Fig. 1 Level diagram with ^{171}Yb for the two theories of selectively exciting one ($|1\rangle$) of two nuclear spin qubit states $|0(1)\rangle$ to the Rydberg state $|r\rangle$. **(a)** Theory 1: When a megahertz-scale frequency separation Δ between the two transitions $|0\rangle \leftrightarrow |r\rangle$ and $|1\rangle \leftrightarrow |r\rangle$ arises from a magnetic field, and when the Rabi frequency Ω for $|1\rangle \leftrightarrow |r\rangle$ satisfies the condition $\bar{\Omega} = \sqrt{\Omega^2 + \Delta^2} = 2N\Omega$ with an integer N (if the Rydberg Rabi frequencies on both qubits are equal), a π pulse excites $|1\rangle$ to $|r\rangle$, but meanwhile the input state $|0\rangle$ undergoes N cycles of detuned Rabi rotation, returning to itself. **(b)** Theory 2: A two-photon excitation via the lowest 3P_1 state can be tuned resonant to a 3S_1 Rydberg state. Due to selection rules, only the nuclear spin state $m_F = -1/2$ is excited to the Rydberg state. The level diagram is not to scale. Theory 2 is applicable even if the mismatch of the transition frequencies for $|0(1)\rangle \leftrightarrow |r\rangle$ is negligible.

given to selectively and rapidly transfer one nuclear spin qubit state from the ground state to a Rydberg state of an AEL atom. For Theory 1 shown in Fig. 1(a), a magnetic field B on the order of 0.1 mT for specifying the quantization axis splits the degeneracy of the two transitions $|0\rangle \leftrightarrow |r\rangle$ and $|1\rangle \leftrightarrow |r\rangle$ with a frequency mismatch Δ on the order of megahertz. A megahertz-rate Rabi flopping between ground and Rydberg states is required to avoid decoherence in the Rydberg states, so the Rabi frequency Ω for the rotation $|1\rangle \leftrightarrow |r\rangle$ should be on the order of megahertz, leading to an undesired detuned Rabi oscillation between $|0\rangle$ and $|r\rangle$. The generalized Rabi frequency $\bar{\Omega}$ for the detuned Rabi oscillation of $|0\rangle$ is $\sqrt{\Omega^2 + \Delta^2}$ [34], and, remarkably, the condition $\bar{\Omega}/\Omega = 2N$ can lead to N cycles for the detuned Rabi rotations between $|0\rangle$ and $|r\rangle$ when $|1\rangle$ is excited to $|r\rangle$, where N is an integer. Although there is a phase accumulation in $|0\rangle$, it can be canceled by single-qubit phase gates for designing a controlled-Z (C_Z) gate as shown later. For Theory 2 shown in Fig. 1(b), a two-photon Rydberg excitation $|1\rangle \rightarrow |r\rangle$ is achieved via circularly polarized laser fields. We show by realistic data that it is possible to choose appropriate intermediate states and Rydberg states so that we can completely suppress the Rydberg excitation of $|0\rangle$ when $|1\rangle$ is excited

to Rydberg states. Theory 2 does not rely on a MHz-scale Δ and, in fact, any value of Δ is fine. Theory 2 can also be executed by pulse-shaping methods such as stimulated Raman adiabatic passage (STIRAP) [35–37] that are useful for Rydberg atom quantum entanglement [8, 22, 38–64]. In comparison, Theory 1 cannot be implemented with STIRAP, but it can be used with one-photon excitation of p -orbital Rydberg states [18, 65].

After reviewing the present stage of AEL-based quantum computing in Section 2, we detail our theories with ytterbium in Section 3 and briefly study strontium in Section 4 because these two elements are well studied in experiments, as shown in Refs. [27, 28, 33] and [25, 29–31, 66], respectively. Discussions and conclusions are given in Section 5 and 6, respectively. Although Section 3 contains necessary details, more are grouped in the appendixes to avoid blurring the essence of the theories.

2 Nuclear spin states as qubit states

2.1 A brief review of previous methods

It will be useful to briefly review previous gate proposals with AEL atoms. The motivation is that they have stable nuclear spin states which can be used to store information, and there can be collisional interaction that enables entanglement [67–69]. Moreover, for elements with nonzero nuclear spins, an electric singlet-triplet clock transition from the ground state can be decoupled from the nuclear spin. As a consequence, the atoms can be cooled without changing the quantum states of the nuclear spin, which is an awesome benefit to store the information in the state space of the nuclear spin [32]. This in principle means that when qubits heat up after many cycles of quantum control as required in quantum computing, they can be cooled again without changing the information stored in the quantum system. Although there is only one ground level 1S_0 for well studied AEL atoms, their first excited 3P_0 state has a long lifetime τ , which can be used for shelving one of the nuclear spin qubit states for information readout; for the case of ytterbium studied in this work, τ is about 26 s [70] which can exceed the time scale of relevant quantum control by many times. Besides, coding information in the nuclear spin states can avoid environmental noise such as fluctuation of magnetic fields. These several advantages motivated proposals for entangling atoms with two valence electrons by merging them from different sites for the induction of a blockade or exchange interaction [69, 71], where the latter has been studied in experiments [72–74]. Till now, several theories have been put forward for showing that high-fidelity quantum gates should be feasible via the collisional interaction [75–79].

Another method is to use the optical clock transition $^1S_0 \leftrightarrow ^3P_0$ of AEL neutral atoms [80], where a qubit

is defined by the electronic ground and long-lived clock states. This method easily offers frequency-selective excitation to Rydberg states. As in the experiment [25], the 3P_0 clock state was coherently and rapidly excited to a Rydberg state, leading to high-fidelity two-atom entanglement between the Rydberg and optical-clock states.

2.2 Difficulties in selective Rydberg excitation of one nuclear spin qubit state

In this work, we show that entanglement between nuclear spins in two-electron atoms can be efficiently generated by Rydberg interactions. Compared to the collisional gates [71, 75–79], our Rydberg gate is implemented on a much shorter microsecond timescale. But there are difficulties to achieve our goal.

The first difficulty is that Rydberg states are not stable. Different isotopes have different properties. We take ^{171}Yb as an example to briefly show the difficulties one by one while more details are grouped in Appendixes A–E. The qubit is defined by two nuclear spin states, $|0(1)\rangle \equiv |(6s^2)^1S_0, m_I = \pm 1/2\rangle$, among which one should be excited to a Rydberg state $|r\rangle \equiv |(6sns)^3S_1, F = I + 1\rangle$ for entanglement generation. As estimated in Appendix C, the lifetime of $|r\rangle$ is about $\tau = 330 \mu\text{s}$ for $n = 70$ at room temperatures. Rydberg excitation should take place within a time much shorter than τ .

The second difficulty is that for frequently studied AEL atoms, there is no hyperfine splitting in the ground states. When laser fields are sent to qubits for exciting $|1\rangle$ to Rydberg states, the other qubit state $|0\rangle$ can also be excited. Moreover, because the dipole matrix elements between the ground state and a Rydberg state is rather tiny, a two-photon Rydberg excitation is more favorable. A standard way to achieve this is to use a largely detuned intermediate p -orbital state $|p\rangle$ for Rydberg excitation. To avoid using ultraviolet light of too short wavelengths, the lowest 1P_1 or $^3P_{0,1,2}$ states can be used as the intermediate state. But for the lowest 1P_1 state whose excitation from the ground state is spin and dipole allowed, it is difficult to find available laser powers to compensate the fast dissipation of 1P_1 . For the lowest $^3P_{0,1,2}$ manifold, it is unclear whether the transition can be fast enough with available technology.

The third difficulty lies in that weak magnetic fields are preferred in experiments when Rydberg states need to be coherently excited. Although strong magnetic fields can in principle lead to a GHz-scale Δ , they are incompatible with Rydberg atom quantum science. First, Rydberg excitation of neutral atoms requires sending laser fields to the vacuum chamber in various directions that cause trouble in setting up devices for generating strong magnetic fields. Second, qubits are often left in free flight during Rydberg excitation so that an inhomogeneous distribution of \mathbf{B} leads to an extra dephasing [81, 82], and the gradient of \mathbf{B} along the motional direction of the qubits can be larger

when stronger fields are employed. The magnitudes of \mathbf{B} in Rydberg gate experiments by alkali-metal atoms were 9, 11.5, 3.7, 1.5, 4.8, 3, 1.5, 7.5, 8.5, and 6 G in Ref. [14–23], respectively. In a recent experiment with AEL qubits, a 710 G field was used for state initialization [25], but \mathbf{B} was switched to 71 G during Rydberg excitation [25].

3 Selective Rydberg excitation of a nuclear spin state of ^{171}Yb

3.1 Theory 1

Theory 1 is shown in Fig. 1(a) with π polarized laser fields where $|1\rangle$ is resonantly excited. The complicated level scheme of AEL requires extra efforts to design the scheme to excite a nuclear spin state.

For ^{171}Yb , there is no quadrupole interaction, and the Hamiltonian for the Zeeman interaction in the presence of a magnetic field \mathbf{B} is

$$\hat{H} = A\hat{\mathbf{I}} \cdot \hat{\mathbf{J}} + \mathbf{B} \cdot (g_J\mu_B\hat{\mathbf{J}} - g_I\mu_n\hat{\mathbf{I}}), \quad (1)$$

where A is the nuclear magnetic dipole constant, $\hat{\mathbf{I}}$ and $\hat{\mathbf{J}}$ are the nuclear and electron spin operators, respectively, and $g_{I(J)}$ is the nuclear (electron) g factor. Here, μ_B is the Bohr magneton and μ_n is the nuclear magneton, which is equal to $\mu_n = 0.4919\mu_N$ for ^{171}Yb [83] and $\mu_N \approx \mu_B/1836$. Because different electron orbits have different contacts with the nucleus, different states have different values of A [84–87]. For the ground state the total electron angular momentum is zero, and the only term left in Eq. (1) is the Zeeman splitting $g_I\mu_n B_z$ between $|0\rangle$ and $|1\rangle$. Larger fields can be used for optical pumping during the state initialization, afterward the field can be lowered, as in Ref. [25]. $A/(2\pi)$ is 3.958 GHz [88] for the $(6s6p)^3P_1$ state, and is -0.21 GHz [87] for the $(6s6p)^1P_1$ state (the sign of A is delicate in that some previous measurement suggested a positive A [84]). For a highly excited Rydberg electron, its contact with the nucleus is negligible, and the hyperfine interaction of the Rydberg atom is mainly between the nucleus and the inner valence electron, with $A/(2\pi) \approx 12.6$ GHz according to the measurement in Ref. [89]. With $n \approx 70$, the analysis in Appendix B shows that $A\hat{\mathbf{I}} \cdot \hat{\mathbf{J}}$ couples the $|(6sns)^1S_0, F = I\rangle$ and $|(6sns)^3S_1, F = I\rangle$ states (when $F = 1/2$) to form two new eigenstates $|\lambda_{\pm}\rangle$ while $|\lambda_0\rangle = |(6sns)^3S_1, F = I + 1\rangle$ remains uncoupled. This leads to three states $\{|\lambda_0\rangle, |\lambda_+\rangle, |\lambda_-\rangle\}$ with energies $2\pi \times (6.3, 4.8, -6.1)$ GHz in reference to the unperturbed energy of the ^{174}Yb $|(6sns)^1S_0\rangle$ state. For $n \sim 70$, Appendix B shows that when we choose $|\lambda_+\rangle$ as $|r\rangle$ a MHz-scale Rydberg Rabi frequency can safely avoid the leakage to other nearby states.

An appropriate intermediate state must have two properties. First, it should possess balanced dipole matrix elements to the ground and Rydberg states. Second,

large enough laser power at the transition wavelengths should be available to realize coherent excitations. Several choices are at hand. The $(6s6p)^1P_1$ state, which is $2\pi \times 751.5$ THz over the ground state, can have a strong coupling with the ground state, but it has a short lifetime about 5 ns [90]. To avoid dissipation from the intermediate state, it should be largely detuned, which makes it challenging to achieve a MHz-scale two-photon Rydberg Rabi frequency. A similar issue exists for $(6s7p)^1P_1$, which is $2\pi \times 1216.1$ THz over the ground state and has a short lifetime about 10 ns. The $(6s6p)^3P_1$ state is $2\pi \times 539.4$ THz over the ground state and has a lifetime about 800 ns [90]. This makes it a useful choice because a smaller detuning at the intermediate state is enough, so that a MHz-scale two-photon Rabi frequency becomes possible as shown in Appendix D. In principle, the clock state cannot be coupled with the ground state, but due to mixing with the $(6s6p)^1P_1^0$ by spin-orbit interaction [91] that results in (see Appendix A)

$$|(6s6p)^3P_1\rangle = a|(6s6p)^3P_1^0\rangle + b|(6s6p)^1P_1^0\rangle, \quad (2)$$

it becomes possible to be coupled to the ground state, where the superscript 0 denotes pure Russell-Saunders coupling and $(a, b) = (0.991, -0.133)$ [92].

The spin-orbit coupled state in Eq. (2) is the key feature that enables our theories. The dipole matrix element between the ground (Rydberg, with $n = 70$) and the intermediate states is on the order of $0.1 (10^{-3})ea_0$, as shown in Appendixes B, C, and D. So, fast enough Rabi rotation between the qubit state and $|(6s6p)^3P_1\rangle$ is feasible even though $|b|$ is only 0.133. On the other hand, a is near 1, and the dipole coupling between $|(6s6p)^3P_1\rangle$ and $|r\rangle$ can reach a large value for $n = 70$. The laser wavelengths of about 556 and 308 nm for the lower and upper transitions in Fig. 1 are available with commercial or homemade lasers, where the 556 nm light source has been widely used in spectroscopy [88, 93] or atomic trapping and cooling [28, 31, 94]. As for the UV lasers [14, 65], laser systems with wavelengths tunable in the range 304–309 nm [95] were frequently used for exciting Rydberg states of a strontium ion [95–97]. Detailed analysis in Appendix D shows that with technically available resources, the effective Rabi frequency between $|1\rangle$ and $|r\rangle$ can be $\Omega_{1r}/(2\pi) = 1.4$ MHz, and meanwhile the Rabi frequency for the transition between $|0\rangle$ and $|r'\rangle = (6s70s)^3S_1 F = 3/2, m_F = 1/2$ is $-\Omega_{1r}$.

A π pulse with duration t_π can complete the transition $|1\rangle \rightarrow -i|r\rangle$. To avoid exciting $|0\rangle$ to the Rydberg state, it is desirable to realize a generalized Rabi frequency $\bar{\Omega} = \sqrt{\Omega_{1r}^2 + \Delta^2}$ which is $2N$ times Ω_{1r} , where N is an integer. As can be easily proved [34, 98], with a duration t_π of the Rydberg lasers, the input state $|0\rangle$ undergoes N detuned Rabi cycles, evolving to

$$|0\rangle \rightarrow e^{i\alpha}|0\rangle, \quad (3)$$

where $\alpha \equiv -[N + \Delta/(2\Omega_{1r})]\pi$. Note that to implement the Rydberg gate with Rydberg interaction V , there is

a phase shift $\beta = \pi|\Omega_{1r}|/(2V)$ to the input state $|1\rangle$ because of the blockade error as studied in Refs. [99, 100], extra phase shifts to the laser fields are required to recover a controlled-Z (C_Z) gate. More than that, because when the control qubit state $|1\rangle$ is excited to $|r\rangle$, the off-resonant excitation of $|0\rangle$ to $|r'\rangle$ in the target qubit results in a similar phase shift $\beta' = \pi|\Omega_{1r}|/[2(V + \Delta)]$ for the two-qubit input state $|10\rangle$. So, based on the Rydberg blockade gate and following Ref. [99], we modify the standard $\pi - 2\pi - \pi$ pulse sequence of Ref. [8] by replacing the 2π pulse on the target qubit with two π pulses, where the latter π pulse has a phase shift 2α relative to the first one. Then, we realize the state transform

$$\begin{aligned} |00\rangle &\rightarrow e^{i4\alpha}|00\rangle, \\ |01\rangle &\rightarrow -e^{i4\alpha}|01\rangle, \\ |10\rangle &\rightarrow -e^{i\beta'}|10\rangle, \\ |11\rangle &\rightarrow -e^{i\beta}|11\rangle. \end{aligned} \quad (4)$$

Afterwards, single-qubit phase gates can be applied to the control qubit for $|0\rangle \rightarrow e^{-i4\alpha}|0\rangle$ and $|1\rangle \rightarrow e^{-i\beta}|1\rangle$ so that a quasi controlled-Z (C_Z) gate is realized with the gate matrix $U = \text{diag}\{1, -1, -e^{i(\beta' - \beta)}, -1\}$, which differs a little bit from the standard Rydberg C_Z gate $\mathcal{U} = \text{diag}\{1, -1, -1, -1\}$. In the standard Rydberg blockade gate [10] studied here, we need $V \gg \Omega_{1r}$, so $\beta' - \beta$ is a tiny number because $\Delta \sim \Omega_{1r}$. Averaging equally over the four possible input states $|00\rangle, |01\rangle, |10\rangle$, and $|11\rangle$ and using the fidelity formula in Ref. [101],

$$\frac{1}{20} [|\text{Tr}(U^\dagger \mathcal{U})|^2 + \text{Tr}(U^\dagger \mathcal{U} \mathcal{U}^\dagger U)], \quad (5)$$

the error due to different phases accumulated in $|10\rangle$ and $|11\rangle$ is

$$\begin{aligned} E_{\text{ph}} &= 0.3[1 - \cos(\beta' - \beta)] \\ &\approx 0.15(\beta' - \beta)^2. \end{aligned} \quad (6)$$

The error in Eq. (6) is less than 10^{-5} for the parameters shown later.

Theory 1 can be realized with small magnetic fields. To have, for example, $N = 2$, a magnetic field $B \approx 3.9$ G (we use $g_J = g_L$ for brevity; the g factor depends on the choice of $|r\rangle$ shown in Appendix B) can be used to induce a Zeeman shift $\Delta = \sqrt{15}\Omega_{1r}$, so that the generalized Rabi frequency $\bar{\Omega} = \sqrt{\Omega_{1r}^2 + \Delta^2} = 4\Omega_{1r}$ is realized. The smallness of B is of vital importance since during Rydberg excitation the qubit is released, experiencing free flight and, hence, different magnetic fields. The smaller the magnetic field generated, the smaller its fluctuation.

3.2 Theory 2

Theory 2 is shown in Fig. 1(b) where the same symbol $|r\rangle$ is used though m_F is different from that in Fig. 1(a). The two-photon transition $|1\rangle \rightarrow |r\rangle$ is resonant with right-hand polarized fields. As a consequence there is no way to

couple $|0\rangle$ to $(6s70s)^3S_1$ since it does not have a $m_F = 5/2$ state. As shown in Appendix E, the angular coupling coefficients for $|1\rangle \rightarrow |r\rangle$ are $\sqrt{3}$ times those in Section 3.1. This basically means that if the field amplitudes are the same for the corresponding lasers used in Figs. 1(a) and (b), the achievable Rabi frequency for exciting $|1\rangle$ to $|r\rangle$ can be $\Omega_{1r}/(2\pi) = 2.4$ MHz, leading to a Rydberg-state decay error $7\pi/(4\Omega_{1r}) \approx 1.1 \times 10^{-3}$. Because there is a phase shift to $|11\rangle$ due to the imperfect blockade, we follow Ref. [99] to modify the standard $\pi - 2\pi - \pi$ pulse sequence of Ref. [8] by replacing the 2π pulse on the target qubit with two π pulses, where the second pulse has a phase shift β relative to the first one. Moreover, as shown later, because the qubit state $|0\rangle$ undergoes highly off-resonant excitation to the intermediate state, there is a certain phase accumulation θ in $|0\rangle$ for each π pulse used for $|1\rangle \leftrightarrow |r\rangle$. Then, Theory 2 can realize the gate

$$\begin{aligned} |00\rangle &\rightarrow e^{i4\theta}|00\rangle, \\ |01\rangle &\rightarrow -e^{i(2\theta+\beta)}|01\rangle, \\ |10\rangle &\rightarrow -e^{i2\theta}|10\rangle, \\ |11\rangle &\rightarrow -e^{i\beta}|11\rangle, \end{aligned} \quad (7)$$

where $\theta \approx 0.084\pi$ as shown later in Section 3.3 and Fig. 3(b). Different from Eq. (4), the state $|10\rangle$ does not have a blockade-induced phase shift because the qubit state $|0\rangle$ can only be excited to the largely detuned intermediate state. Single-qubit phase gates can be applied to both qubits for the transform $|0\rangle \rightarrow e^{-i2\theta}|0\rangle$, and an extra single qubit gate $|1\rangle \rightarrow e^{-i\beta}|1\rangle$ can be applied to the target qubit to recover a C_Z gate. The gate by Theory 2 has no phase error as in Eq. (6).

Theory 2 differs from Theory 1 in that there is a highly off-resonant excitation from $|0\rangle$ to the intermediate 3P_1 state. With the estimate in Appendix E, the ratio between the single-photon Rabi frequency and the detuning to the intermediate state is about 0.01, which leads to an error less than 5×10^{-5} due to the scattering at 3P_1 .

The gates in Eqs. (4) and (7) rely on the Rydberg blockade mechanism. To estimate the van der Waals interaction between AEL Rydberg atoms [102], we use quantum defects in Ref. [103] and radial integration of Ref. [104], and calculate [105] $C_6/(2\pi) = 32$ GHz $\cdot\mu\text{m}^6$ for two $(6s70s)^1S_0$ atoms lying along the quantization axis. The interaction for atoms in the 3S_1 states should be much larger because they have nine dipole-dipole transition channels for each set of principal quantum numbers, while two atoms in 1S_0 only have one, i.e., it couples with $|{}^1P_1^1P_1\rangle$. But the quantum defects for the ${}^3P_{0,1,2}$ Rydberg states of ytterbium are not available. To have a conservative estimate (also because we can choose either $(6s70s)^3S_1$ or $|r\rangle$ as $|r\rangle$, see Appendix B), we suppose that the C_6 coefficient of $|r\rangle$ is only six times that of $(6s70s)^1S_0$, and, thus, with a qubit spacing 4 μm , the interaction is $V = 2\pi \times 47$ MHz, which can validate the blockade mechanism with $\Omega_{1r}/(2\pi) = 1.4$ (2.4) MHz in Eqs. (4) [(7)]

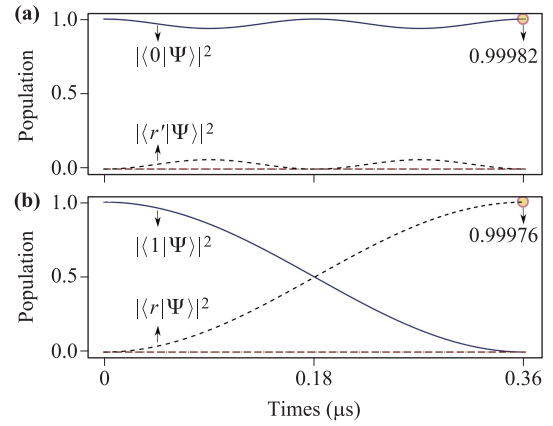


Fig. 2 Population evolutions by Theory 1 for the input states $|0\rangle$ and $|1\rangle$ in (a) and (b), respectively. The solid (short dashed) curve denotes population in the qubit (Rydberg) state, and the dash-dotted and long dashed curves show populations in the two intermediate states $|1(3)/2\rangle$. In both (a) and (b), the populations in $|1(3)/2\rangle$ are on the order of 10^{-4} or below during the pulse. The simulations were done with Eq. (11) and Eq. (10), respectively, with parameters specified in the texts near them. The final populations in $|0\rangle$ of (a) and in $|1\rangle$ of (b) are respectively 0.9995 and 0.9994 at $t = t_\pi$. But we find that at the moment $t = t_o \equiv 0.9994t_\pi$, the populations are 0.99982 and 0.99976, respectively. So the pulse duration $0.9994t_\pi$ is better. Also, the phase error is negligible. At $t = t_o$ the value $\arg\langle 0|\Psi\rangle$ differs from the angle α in Eq. (3) (with $N = 2$) by only $6.0\pi \times 10^{-6}$ in (a), and the phase error in (b) is negligible, $1/2 - \arg\langle 1|\Psi\rangle/\pi = 6.5 \times 10^{-5}$.

with a blockade error [81]

$$E_{\text{bl}} = (\Omega_{1r}^2/8)[1/V^2 + 1/(V + \Delta)^2], \quad (8)$$

for Theory 1, and

$$E_{\text{bl}} = \Omega_{1r}^2/(8V^2), \quad (9)$$

for Theory 2. That there is an extra blockade error in Eq. (8) is because for Theory 1, the input state $|10\rangle$ also experiences blocked Rydberg excitation, but with a detuning $V + \Delta$. Then, we find that E_{bl} is about 2.0 (3.3) $\times 10^{-4}$ for Theory 1 (2).

3.3 Numerical test

The Hamiltonian for the input state $|1\rangle$ in Theory 1 is

$$\hat{H}_1 = \frac{1}{2} \begin{pmatrix} 2\mathbb{D}_r & \Omega_3^{(1)} & \Omega_1^{(1)} & 0 \\ \Omega_3^{(1)} & 2\delta_1 + 2\delta_2 & 0 & \omega_3^{(1)} \\ \Omega_1^{(1)} & 0 & 2\delta_1 & \omega_1^{(1)} \\ 0 & \omega_3^{(1)} & \omega_1^{(1)} & 2\mathbb{D}_1 \end{pmatrix} \quad (10)$$

written in the basis $\{|r\rangle, |3/2\rangle, |1/2\rangle, |1\rangle\}$ where $|r\rangle \equiv |(6s70s)^3S_1, F = 3/2, m_F = -1/2\rangle$, and $|3(1)/2\rangle$ are the shorthand notations for the states $|(6s6p)^3P_1, F = 3(1)/2, m_F = -1/2\rangle$. Here, δ_1 is the detuning given

by the frequency of the lower laser field minus the frequency of the atomic transition and $-\delta_2$ is the hyperfine gap of 3P_1 . The pulse duration is $t_\pi = \pi/\Omega_{1r}$, where $\Omega_{1r} = \frac{\omega_1^{(1)}\Omega_1^{(1)}}{2\delta_1} + \frac{\omega_3^{(1)}\Omega_3^{(1)}}{2(\delta_1+\delta_2)}$. With experimentally achievable laser field strengths as specified in Appendix D, we can have $(\omega_1^{(1)}, \Omega_1^{(1)}, \delta_1)/(2\pi) = (-39.9, 103, 2970)$ MHz, $\delta_2 = -2\delta_1$, $\omega_3^{(1)} = \sqrt{2}\omega_1^{(1)}$, $\Omega_3^{(1)} = -\Omega_1^{(1)}/\sqrt{2}$. Because the adiabatic elimination of the intermediate states, there will be Stark shifts for the states $|1\rangle$ and $|r\rangle$. To compensate them, we assume that careful calibration is made by, e.g., adding extra highly off-resonant fields [17, 106], to induce effective shifts $\mathbb{D}_1 = -(\omega_1^{(1)})^2/(4\delta_1)$ and $\mathbb{D}_r = (\Omega_1^{(1)})^2/(8\delta_1)$.

The Hamiltonian for the input state $|0\rangle$ is

$$\hat{H}_0 = \frac{1}{2} \begin{pmatrix} 2(\mathbb{D}_r + \Delta) & |\Omega_3^{(1)}| & |\Omega_1^{(1)}| & 0 \\ |\Omega_3^{(1)}| & 2\delta_1 + 2\delta_2 & 0 & |\omega_3^{(1)}| \\ |\Omega_1^{(1)}| & 0 & 2\delta_1 & -|\omega_1^{(1)}| \\ 0 & |\omega_3^{(1)}| & -|\omega_1^{(1)}| & 2\mathbb{D}_1 \end{pmatrix} \quad (11)$$

in the basis $\{|r'\rangle, |3/2\rangle, |1/2\rangle, |1\rangle\}$. Here, $\Delta = \sqrt{15}\Omega_{1r}$ denotes the Zeeman shift between the states $|r'\rangle$ and $|r\rangle$ from a magnetic field about 3.9 G; the tiny Zeeman shift between $|0\rangle$ and $|1\rangle$ is absorbed in Δ in the rotating frame transformation, and the Zeeman shifts in the intermediate states are small compared to the hyperfine gap, and, thus,

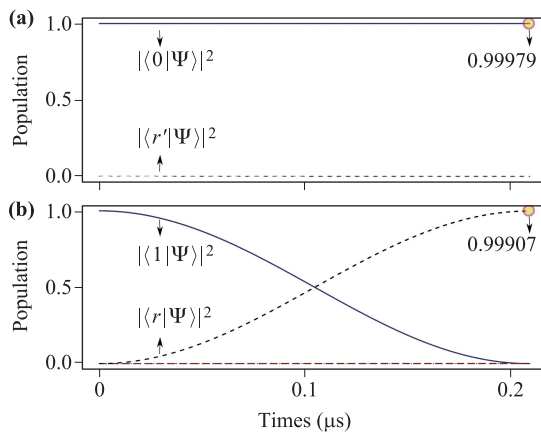


Fig. 3 Population evolutions by Theory 2 for the input states $|0\rangle$ and $|1\rangle$ in (a) and (b), respectively. The solid (short dashed) curve denotes population in the qubit (Rydberg) state, and the dash-dotted and long dashed curves show populations in the two intermediate states $|1(3/2)\rangle$. The simulation in (b) was done with Eq. (10) with parameters specified in the texts near the end of Section 3. The final populations in $|0\rangle$ of (a) and in $|1\rangle$ of (b) are respectively 0.99983 and 0.99821 at $t = t_\pi$. But we find that at the moment $t = t_o \equiv 0.9994t_\pi$, the populations are 0.99979 and 0.99907, respectively. Thus the pulse duration $0.9994t_\pi$ is better as in Fig. 2. The phase error is negligible in (b), with $\arg\langle 1|\Psi\rangle/\pi - 1/2 = 8.9 \times 10^{-5}$ at $t = t_o$. However, there is a phase $\arg\langle 0|\Psi\rangle/\pi = -0.084$ at $t = t_o$ in (a).

are neglected. Details for deriving Eqs. (10) and (11) are given in Appendix D.

Figure 2 shows the simulation results with Eqs. (10) and (11). With a pulse duration t_π , the population transfer is not as accurate as expected because the detunings at the intermediate states $|1(3/2)\rangle$ are finite. But with a pulse duration $t_o = 0.9994t_\pi$, the population transfer from $|1\rangle$ to $|r\rangle$ has a fidelity 0.99976, and meanwhile the population in $|0\rangle$ remains there with a fidelity 0.99982. After the excitation process shown in Fig. 2, another pulse of the same duration t_o can be used so that the initial states are restored with fidelities 0.99961 and 0.99984 for $|0\rangle$ and $|1\rangle$, respectively. The bizarre fact that the population error in $|1\rangle$ is not twice of the error in the transition $|1\rangle \rightarrow |r\rangle$ results from a peculiar interference between the different transition pathways. The average Rydberg superposition time is $(\pi/4)(7/\Omega_{1r} + 3\Omega_{1r}/\bar{\omega}^2)$, leading to a decay error about 1.9×10^{-3} with $\Omega_{1r}/(2\pi) = 1.4$ MHz and $\tau = 330 \mu\text{s}$. With the phase error in Eq. (6), blockade error in Eq. (8), intrinsic rotation error, and the Rydberg-state decay, the infidelity of the C_Z gate is 2.4×10^{-3} which is dominated by the Rydberg-state decay. To have a fidelity beyond 0.999, our results suggest that to host qubits in cryogenic chambers is necessary.

In Theory 2, the Hamiltonian for the input state $|1\rangle$ is still Eq. (10) but with different parameters because circularly polarized fields are used in Fig 1(b) as detailed in Appendix E. With similar strengths of laser fields used in the simulation for Fig. 2, we have $(\omega_1^{(1)}, \Omega_1^{(1)}, \delta_1)/(2\pi) = (56.4, 126, 2970)$ MHz, $\delta_2 = -2\delta_1$, $\omega_3^{(1)} = \omega_1^{(1)}/\sqrt{2}$, $\Omega_3^{(1)} = -\sqrt{2}\Omega_1^{(1)}$. The required extra detunings at the ground and Rydberg states are $\mathbb{D}_1 = (\omega_1^{(1)})^2/(8\delta_1)$ and $\mathbb{D}_r = -(\Omega_1^{(1)})^2/(4\delta_1)$, respectively. For the input state $|0\rangle$, it is excited to $|3/2\rangle$ with detuning $\delta_1 + \delta_2$ and Rabi frequency $\omega_3^{(1)} = 2\pi \times 49$ MHz. By these parameters, the population dynamics for the two input states $|0(1)\rangle$ are shown in Fig. 3. As in Fig. 2, we find that a pulse duration $t_o = 0.9994t_\pi$, instead of t_π , can lead to a more accurate Rydberg excitation. In sharp contrast to Theory 1, the phase accumulation in the input state $|0\rangle$ cannot be neglected. At the end of the pulse we find $\arg\langle 0|\Psi\rangle/\pi = -0.084$. This phase is accumulated due to the detuned Rabi oscillation between the ground state and the intermediate state $|3/2\rangle$ with a generalized Rabi frequency $\bar{\omega} \equiv \sqrt{(\omega_3^{(1)})^2 + (\delta_1 + \delta_2)^2}$ [34, 98]. The phase is accumulated in a way similar to that in Eq. (3), but with a much larger $\bar{\omega}$. In each generalized Rabi cycle, there is a phase accumulation $-\pi[1 + (\delta_1 + \delta_2)/\bar{\omega}]$, leading to $\pi(\delta_1 + \delta_2 + \bar{\omega})/|\Omega_{1r}| \approx -0.084\pi$ for a pulse duration $\pi/|\Omega_{1r}|$. This extra phase in $|0\rangle$ can be effectively eliminated by the single-qubit phase gates as shown below Eq. (7). So, including the blockade error in Eq. (9), the intrinsic rotation error, and the Rydberg-state decay, the infidelity of the C_Z gate by Theory 2 is 2.0×10^{-3} that is again dominated by the Rydberg-state decay.

3.4 Gate error due to the fluctuation of magnetic fields

The fluctuation of magnetic fields can cause frequency jitter in the atomic transitions between the ground, intermediate, and Rydberg states. Both the two qubit states have zero electron angular momentum, and the g factor is simply that of the nuclear spin. Because the nuclear magneton is about 1836 times smaller than the Bohr magneton, the level shifts in the qubit states can be neglected when estimating the gate error from the field fluctuation.

When the magnetic field is exactly equal to the value we desire, the Hamiltonians for the states $|1\rangle$ and $|0\rangle$ are described by Eqs. (10) and (11), respectively. With a fluctuation σ_B of the magnetic field, Eqs. (10) and (11) become

$$\text{Eq.(10)} - \text{diag}\{g_R, g_i, g_i, g_g\}\sigma_B\mu_B/2, \quad (12)$$

and

$$\text{Eq.(11)} + \text{diag}\{g_R, g_i, g_i, g_g\}\sigma_B\mu_B/2, \quad (13)$$

respectively, where the subscripts R , i , and g distinguish the Rydberg, intermediate, and ground states, and the minus and plus signs in the two lines above originate from the two different Zeeman levels associated with the two qubit states. As discussed above, we set $g_g = 0$ here since the nuclear spin Zeeman splitting is tiny compared to those of the electrons. The Rydberg g factor g_R depends on the state we choose, shown in Appendix B. For brevity, we take $g_R = 1$ as an example. The g factors for the two intermediate states should be calculated according to the mixing between the singlet and triplet states shown in Eq. (2), $g_p = a^2g(^3P_1) + b^2g(^1P_1) \approx 1.49$ [107–109], where $g(^3P_1)$ and $g(^1P_1)$ are 1.5 and 1, respectively.

To quantify the error from the magnetic field fluctuation, we use Eq. (5) by defining \mathcal{U} as the ideal gate matrix, and calculate U for each nonzero σ_B . In the Rydberg blockade gate [8, 10], the blockade error is estimated by averaging gate errors with interactions varying around the desired V . This is because the blockade error can accidentally vanish [58] for a certain V that depends on the impossible condition of absolutely static atoms. Thus, we

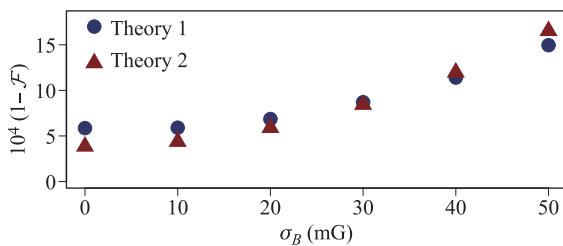


Fig. 4 Gate error (scaled by 10^4) due to the fluctuation of magnetic field σ_B in units of mG ($=10^{-7}$ T). Round (rectangular) symbols denote results for Theory 1 (2). The numerical evaluation assumes perfect Rydberg blockade via Eqs. (10)–(13) with the gate fidelity defined in Eq. (5).

use Eq. (8) for a useful estimate of the blockade error but assume large enough V here to estimate the error solely from σ_B .

Numerical results with σ_B up to 50 mG are shown in Fig. 4, where the round (rectangular) symbols denote results for Theory 1 (2). One can see that when no field fluctuation occurs, the rotation error is about 5×10^{-4} . This is because as shown in Figs. 2 and 3, there are intrinsic rotation errors in the two-photon Rydberg excitations. Figure 4 shows that with a field fluctuation around 10 mG, the rotation error is nearly the same as when there is no field fluctuation. As shown in the Supplemental Materials of Ref. [23], $\sigma_B < 10$ mG is achievable with $B = 6$ G that is of similar magnitude as used here. Even with a large fluctuation $\sigma_B = 50$ mG, Fig. 4 shows that our method enables a fidelity over 0.996 for both Theory 1 and Theory 2 when including the phase error in Eq. (6), the blockade error in Eq. (8), and the Rydberg-state decay.

4 Rydberg excitation of nuclear spin qubits with ^{87}Sr

It is useful to extend our theories to the case of ^{87}Sr which was widely studied in experiments [25, 29–31, 66, 110–114] and theories [91, 102, 115–120]. Because of the different quantum defects in ytterbium and strontium [116], we calculate that the C_6 coefficient of strontium is 20 times that of ytterbium for a certain 1S_0 Rydberg state. Thus it is possible to set a larger qubit spacing if strontium atoms are used for Rydberg blockade so as to have less crosstalk in the Rydberg lasers. Indeed, the Rydberg blockade interaction of both cold and hot strontium atoms have been experimentally studied [25, 121–123], demonstrating the applicability of strontium in Rydberg atom quantum science.

The key to the shown theories in Section 3 is the hyperfine interactions and spin–orbit couplings. However, such interactions are strikingly different for different AEL atoms. For ^{87}Sr with $I = 9/2$, the qubit states to encode information can be chosen from the states $m_I = 7/2$ and $9/2$, whose degeneracy can be split by a field of the order of 1 G that leads to a kHz-scale Zeeman shift with a nuclear magnetic moment $-1.0936\mu_N$ [124]. To coherently excite the nuclear spin states to Rydberg states, however, we find that the lowest 3P_1 state is no longer the best choice for the intermediate state. This is because for strontium, Eq. (2) becomes

$$|(5s5p)^3P_1\rangle = a|(5s5p)^3P_1^0\rangle + b|(5s5p)^1P_1^0\rangle, \quad (14)$$

with $b = -0.0286$ [91], which is about five times smaller than that for ytterbium. This leads to a rather small Rabi frequency if laser fields of similar magnitudes to those in Section 3 are used.

One solution to the above issue is to use the state $|(5s6p)^1P_1\rangle$ as the intermediate state which can be coupled

to the 1S_0 Rydberg states. As detailed in Appendix F, $|(5s6p)^1P_1\rangle$ has a linewidth $\Gamma = 2\pi \times 0.3$ MHz and it can be coupled to the ground state with a dipole matrix element that is about half of $\langle (6s6p)^3P_1 || er || (6s^2)^1S_0 \rangle$ of ytterbium. If we choose the $|(5s70s)^1S_0\rangle$ state as $|r\rangle$ to entangle the qubits, the achievable Rabi frequencies for $|1\rangle \rightarrow |r\rangle$ are 0.8 times those in Fig. 1 if the same values $\delta_{1(2)} \sim 2\pi \times 3$ GHz are used. In principle, larger Rydberg Rabi frequencies can be achieved by using smaller detunings. More details are shown in Appendix F. Finally, we note that although the 1S_0 Rydberg states do not have large Zeeman shifts, they are coupled to the 3S_1 Rydberg states via the hyperfine interaction. Such a coupling induces a large energy separation on the order of the hyperfine constant, so that we can choose one state as $|r\rangle$. The hyperfine induced state mixing was studied in detail in Ref. [114]; see also Appendix B. In this case, a small magnetic field can lead to a MHz-scale Δ by the electron Zeeman shift although there can be a weak diamagnetic effect in the 1S_0 state [125].

We calculate that the van der Waals interaction coefficient for the strontium $(5s70s)^1S_0$ state is $C_6/(2\pi) = -710$ GHz- μm^6 with the quantum defects used in Ref. [116, 119]. Note that if stronger interactions are desired, one can choose the state near $n = 63$ where Förster resonance occurs [119]. With a qubit spacing of 5 μm the interaction is $|V|/(2\pi) = 45$ MHz, which is large enough to validate the blockade gate in the form of Eq. (7). Compared to the ytterbium case studied at the end of Section 3.2, here the qubit spacing is 1 μm larger while the value of V is almost the same. So, using ^{87}Sr is more favorable to avoid crosstalk compared to ^{171}Yb .

5 Discussion

We have studied exciting nuclear spin qubit states to Rydberg states for entanglement generation. As for single-qubit gates, their implementation with nuclear spins in AEL atoms has been studied in, e.g., Refs. [71, 78, 80]. It is also an open question whether using Rydberg excitation as introduced in this work can we have fast and accurate single-qubit gates. However, a straightforward extension of Theory 1 to single-qubit gate operation is at hand. In the clock transition from the ground 1S_0 state to the lowest 3P_0 state, the transition is possible because there is a small mixing of the $^1P_0^0$ component in the 3P_0 state. A detailed analysis in Ref. [91] shows that with a magnetic field applied there will be a differential shift for the transition $|^1S_0, m_I\rangle \rightarrow |^3P_0, m_I\rangle$ considering different m_I . For the case of ^{87}Sr , the shift is $110 \times m_I \text{ Hz/G}$. This basically means that by applying an appropriate B-field we can excite the two nuclear spin qubit states from the ground state to the 3P_0 state, one resonantly with a kHz-scale Rabi frequency Ω_0 while the other with a generalized Rabi frequency $\bar{\Omega}$ because it is detuned. The detuning can

be specifically set so that $\bar{\Omega}$ is N times Ω , where N is an integer. Then, it is possible to induce single-qubit gates based on the exotic selective excitation of nuclear spin qubits as in Theory 1.

The gates in Eq. (4) for Theory 1 and Eq. (7) for Theory 2 belong to the standard Rydberg blockade gate introduced in Ref. [8]. Based on the Rydberg blockade mechanism, there have been various protocols. For example, simultaneous Rydberg excitation of both qubits can lead to entangling gates in the blockade regime. A special advantage of Theory 1 is that both qubit states experience Rydberg excitation, and different Δ can be easily obtained by different B-fields. It is an open question whether by choosing appropriate ratio between Δ and the Rydberg Rabi frequencies can we generate a C_Z gate with one step. This should be possible since for alkali-metal atoms, fast C_Z -like gates [22] or CNOT gates [106] can be generated with effective one-pulse sequences.

We have based our discussions on the Rydberg blockade mechanism. It is also of interest to extend our theories to Rydberg gates by the antiblockade method [126, 127] as reviewed in Ref. [128]. Although the antiblockade regime is sensitive to the fluctuation of the Rydberg interactions, the simultaneous excitation of both qubit states to Rydberg state, as shown in Theory 1, can be useful for designing exotic logic gates [98]. With short enough Rydberg superposition times, the error from fluctuation of interactions can be small.

6 Conclusions

We provide two theories to realize Rydberg excitation of one of the two nuclear spin ground states of an AEL atom. We perform a detailed study with ytterbium and briefly study strontium when using our theories. The first theory needs an external magnetic field on the order of 1 G to work, while the second method can work also with larger magnetic fields. We have shown methods to realize C_Z gates based on these two theories and found that fidelities over 0.997 are achievable for both methods with feasible resources. The key advantage of our theories is that strong magnetic fields are not required so that fast dephasing from the noises in the magnetic field can be avoided in practical experiments. Because AEL atoms like ytterbium can be easily cooled, can be cooled without altering the information encoded in the nuclear spin space, and their nuclear spins are insensitive to magnetic fluctuations in the environment, our theories can lead to new opportunities for Rydberg atom quantum science and technology.

Acknowledgements The author thanks Yan Lu for insightful discussions. This work was supported by the National Natural Science Foundation of China under Grant Nos. 12074300 and 11805146, the Natural Science Basic Research Plan in Shaanxi Province of China under Grant No. 2020JM-189, and the Fundamental Research Funds

for the Central Universities.

Appendices

A Spin-orbit coupling between the low-lying $^1P_1^0$ and $^3P_1^0$ states

The theory can be easily tested in experiments because the quantum control over alkaline-earth-metal atoms and ytterbium was well studied [25, 27–31]. Here, we give extra details that can be useful to set up laser fields for the excitation scheme shown in the main text. To be specific, we consider ytterbium-171.

There is a spin-orbit coupling between the $|(6s6p)^1P_1^0\rangle$ and $|(6s6p)^3P_1^0\rangle$ states, where the superscript 0 denotes pure Russell-Saunders states. The spin-orbit coupling leads to [91]

$$\begin{aligned} |(6s6p)^1P_1\rangle &= a|(6s6p)^1P_1^0\rangle - b|(6s6p)^3P_1^0\rangle, \\ |(6s6p)^3P_1\rangle &= b|(6s6p)^1P_1^0\rangle + a|(6s6p)^3P_1^0\rangle, \end{aligned} \quad (\text{A1})$$

where (a, b) depend on the atomic species. For ytterbium-171 we have $(a, b) = (0.991, -0.133)$ according to Ref. [92]. For another ytterbium isotope with nuclear spin, i.e., ^{173}Yb , a similar mixing occurs, with $(a, b) = (0.990, -0.141)$ [107].

B Eigenstates with hyperfine splitting

In this appendix we study the hyperfine induced state mixing between the singlet and triplet s -orbital Rydberg states. The hyperfine coupling

$$\hat{V}_{\text{HI}} = A\hat{\mathbf{I}} \cdot \hat{\mathbf{J}} \quad (\text{B1})$$

induces energy shifts [114, 129]

$$\begin{aligned} 0 &= \langle (6sns)^1S_0, F = I | \hat{V}_{\text{HI}} | (6sns)^1S_0, F = I \rangle, \\ -A/2 &= \langle (6sns)^3S_1, F = I | \hat{V}_{\text{HI}} | (6sns)^3S_1, F = I \rangle, \\ A/2 &= \langle (6sns)^3S_1, F = I + 1 | \hat{V}_{\text{HI}} | (6sns)^3S_1, \\ &\quad F = I + 1 \rangle, \end{aligned} \quad (\text{B2})$$

for all cases of AEL atoms, and

$$-A(I + 1)/2 = \langle (6sns)^3S_1, F = I - 1 | \hat{V}_{\text{HI}} | (6sns)^3S_1, \\ F = I - 1 \rangle, \quad (\text{B3})$$

for AEL atoms with $I > 1$.

There is also state mixing between $|(6sns)^1S_0, F = I\rangle$ and $|(6sns)^3S_1, F = I\rangle$. To be specific, we consider ^{171}Yb and label the two states by $|s1\rangle \equiv |(6sns)^1S_0, F = 1/2\rangle$ and $|s2\rangle \equiv |(6sns)^3S_1, F = 1/2\rangle$. For illustration, we consider principal quantum numbers around 70 and study consequences from different n at the end of this section.

The singlet-triplet gap $1.8 \times 10^6/n^{*3}$ GHz between $|s1\rangle$ and $|s2\rangle$ is about $E_s \approx 2\pi \times 5$ GHz with an effective principal quantum number $n^* = 70$. To understand the hyperfine interaction in the state mixing between the two states $|s1\rangle$ and $|s2\rangle$, we follow the method in Refs. [103, 114]. With the energy of ^{174}Yb as a reference, the Hamiltonian for ^{171}Yb is

$$\hat{H}(171) = \hat{H}_0(174, m_{171}) + \hat{V}_{\text{HI}}, \quad (\text{B4})$$

where $\hat{H}_0(174, m_{171})$ is the Hamiltonian of ^{174}Yb rescaled by the isotope shift. Here $m_{171} = m_e M_{171}/(m_e + M_{171})$, where m_e is the mass of an electron and M_{171} is the mass of $^{171}\text{Yb}^+$. In a high-lying Rydberg state, the hyperfine interaction is dominated by the interaction between the inner $6s$ valence electron and the nuclear spin because the highly excited electron is far from the nucleus and, thus, has negligible contact with the nucleus. We take the energy of ^{174}Yb from the eigenenergy of $\hat{H}_0(174, m_{171})$ and treat the hyperfine interaction \hat{V}_{HI} as a perturbation. In the basis of $\{|s2\rangle, |s1\rangle\}$, \hat{V}_{HI} is given by [129]

$$\begin{pmatrix} E_s - A/2 & \sqrt{3}A/4 \\ \sqrt{3}A/4 & 0 \end{pmatrix}, \quad (\text{B5})$$

where A is the nuclear magnetic dipole constant and $E_s \approx 2\pi \times 5$ GHz with $n \sim 70$. According to the measurement in Ref. [89], $A/(2\pi) \approx 12.6$ GHz. Equation (B5) has two eigenstates,

$$|\lambda_{\pm}\rangle \propto [D \mp (E_s - A/2)]|s1\rangle + \sqrt{3}A|s2\rangle/2, \quad (\text{B6})$$

where

$$D = \sqrt{3A^2/4 + (E_s - A/2)^2}, \quad (\text{B7})$$

and the eigenenergies are

$$\lambda_{\pm} = (E_s/2 - A/4) \pm D/2, \quad (\text{B8})$$

which are equal to $2\pi \times 4.8$ and -6.1 GHz, respectively. Then, due to the hyperfine interaction, the energies for the three eigenstates $|(6sns)^3S_1, F = 3/2\rangle$, $|\lambda_+\rangle$, and $|\lambda_-\rangle$ are $2\pi \times (6.3, 4.8, -6.1)$ GHz, respectively, where $2\pi \times 6.3$ MHz is from Eq. (B2). For the purpose in this work, one can choose $|r\rangle = |(6sns)^3S_1, F = 3/2\rangle$ because there will be more states that can be coupled by the dipole-dipole interaction for $|^3S_1\ ^3S_1\rangle$ compared to the state $|^1S_0\ ^1S_0\rangle$, leading to larger van der Waals interactions [116, 119]. For the purpose of state detection it is usually useful to couple Rydberg states to the rapidly decaying low-lying state $(6s6p)^1P_1$. However, with this choice the coupling can be largely limited by the small triplet component in the wavefunction of $(6s6p)^1P_1$ as shown in Eq. (A1).

Another choice is to choose $|\lambda_+\rangle$ as $|r\rangle$. Then, $|\lambda_+\rangle$ is separated from $|(6sns)^3S_1, F = 3/2\rangle$ and $|\lambda_-\rangle$ by $2\pi \times 1.5$ and $2\pi \times 10.9$ GHz, respectively. $|\lambda_+\rangle$ has an amplitude $\langle s2|\lambda_+\rangle \approx -0.66$ in the addressable state $|s2\rangle$ (while $\langle s1|\lambda_+\rangle \approx 0.75$), which should be considered

when estimating the Rabi frequencies. Because the separation between $|r\rangle$ and the other two states is more than $2\pi \times 1.5$ GHz, we can ignore their excitation for a MHz-scale Ω . There is also a mixing between $|(6sns)^1S_0, F = 1/2\rangle$ and $|(6s(n \pm 1)s)^3S_1, F = 1/2\rangle$ with a much smaller coupling constant $\sqrt{3}A/40$ [114]. For $n \sim 70$ considered in this paper, the energy separation between $(6s(n \pm 1)s)^3S_1$ and $(6sns)^3S_1$ is about $2\pi \times 24$ GHz (estimated from the quantum defects of the 1S_0 states [103]), which implies a portion less than 10^{-3} for the states with principal quantum numbers $(n \pm 1)$ in $|\lambda_{\pm}\rangle$. So we can use the description in Eq. (B5).

Note that because $|(6s6p)^3P_1\rangle$ consists of both singlet and triplet states, there is some chance to excite the $|(6s6p)^1P_1^0\rangle$ state to the $|(6snd)^1D_2\rangle$ state. But according to the measured results in [103], the energy of $(6s70s)^1S_0$ is 50417.67cm^{-1} , and the two 1D_2 states nearest to it are $(6s68d)^1D_2$ and $(6s69d)^1D_2$ with energies 50417.33 and 50418.10cm^{-1} , respectively. This means that the gap to the nearest two 1D_2 states from $(6s70s)^1S_0$ is $2\pi \times 10.2$ GHz. Besides, there is some possibility to couple $|(6s6p)^3P_1^0, F = 1(3)/2\rangle$ to the $|(6snd)^3D_{1,2,3}\rangle$ states. But according to the measured results in [103], the energy of $(6s70s)^1S_0$ is 50417.67cm^{-1} , and the two 1D_2 states nearest to it are $(6s68d)^3D_2$ and $(6s69d)^1D_2$ with energies 50417.30 and 50418.07cm^{-1} , respectively; converting to Hz, these two states are away from $(6s70s)^1S_0$ by $2\pi \times (10.2, 12.0)$ GHz. Because the fine gap in high-lying Rydberg states is negligible with $n = 70$, these data show that the state $|r\rangle$ is far separated from nearby states that may be addressed from $(6s6p)^3P_1$.

As a conclusion, we can choose either $|(6sns)^3S_1, F = 3/2\rangle$ or $|\lambda_+\rangle$ as $|r\rangle$. For $n = 70$, the gap to nearby Rydberg states is large if a MHz-scale Rydberg Rabi frequency is employed so that the leakage can be safely neglected. If $|\lambda_+\rangle$ is chosen as $|r\rangle$, the mixing between singlet and triplet states in it means that the Landé factor g_R for the Rydberg state differs from the g factor of the $^3S_1^0$ Rydberg state. With the data shown above, we have $g_R = 2|\langle s2|\lambda_+\rangle|^2 \approx 0.87$. This g factor is more than two times smaller than that of $|(6sns)^3S_1, F = 3/2\rangle$. In order to show numerical examples that can catch the phenomena for both choices of the Rydberg state, we take a value in between with, for example, $g_R = 1$.

C Lifetimes and dipole matrix elements

The lifetimes of high-lying Rydberg states of strontium are not wellknown but can be estimated from measurement results of low-lying Rydberg states. A search in the literature shows that the highest ytterbium Rydberg 1S_0 state whose lifetime was ever measured has a principal quantum number $n = 26$ [130]. The measured lifetimes for the ytterbium 1S_0 Rydberg states with principal quantum numbers $n \in [21, 26]$ show that their lifetimes

are mainly limited by the blackbody radiation at room temperatures [130]. Moreover, Ref. [130] shows that at room temperatures the lifetime is well approximated by $\tau \approx 1.17(n - \mu)^3$ ns for these Rydberg states. According to the recent measurement in [103], we have $\mu \approx 4.278$. By this, we can estimate that the lifetime for the $(6sns)^1S_0$ state is $332 \mu\text{s}$ for $n = 70$.

The achievable Rabi frequency is determined by the dipole matrix elements of the relevant transitions. Because two-photon Rabi frequencies are used, we shall consider both the lower and the upper transitions. In particular, we compare two possible choices with π polarized laser fields (where the r_0 component in the spherical basis is used in the estimate of the dipole matrix elements).

C.1 $(6s6p)^1P_1$ as the intermediate state

The first choice is $(6s^2)^1S_0 \rightarrow (6s6p)^1P_1 \rightarrow (6sns)^1S_0$ with two reduced dipole matrix elements \mathcal{D}_l and \mathcal{D}_u , which are the $^{2S+1}L_J$ -dependent reduced dipole matrix elements for the lower and upper transitions, respectively,

$$\begin{aligned}\mathcal{D}_l &= -\langle (6s6p)^1P_1^0 || er || (6s6s)^1S_0^0 \rangle, \\ \mathcal{D}_u &= -\langle (6sns)^1S_0^0 || er || (6s6p)^1P_1^0 \rangle,\end{aligned}\quad (\text{C1})$$

where e is the elementary charge and the superscript 0 denotes states formed via the ideal Russell–Saunders coupling (otherwise there can be singlet-triplet mixing).

Here, we choose the transition $(6s^2)^1S_0 \rightarrow (6s6p)^1P_1 \rightarrow (6sns)^1S_0$. In principle, we can also consider $(6s^2)^1S_0 \rightarrow (6s6p)^1P_1 \rightarrow (6sns)^3S_1$ since $(6s6p)^1P_1 \rightarrow (6sns)^3S_1$ is possible because the state $(6s6p)^1P_1$ has a $(6s6p)^3P_1^0$ component with a coefficient $-b$ shown in Eq. (A1). However, the dipole coupling to the Rydberg state is already very tiny, and the factor $-b$ is small.

C.2 $(6s6p)^3P_1$ as the intermediate state

The second choice is $(6s^2)^1S_0 \rightarrow (6s6p)^3P_1 \rightarrow (6sns)^3S_1$. However, the transition between singlet and triplet states is spin forbidden. But as shown in Eq. (A1), the state $(6s6p)^3P_1$ has a $(6s6p)^1P_1^0$ component with a coefficient b . The reduced dipole matrix element for the lower transition is still

$$\mathcal{D}_l = -\langle (6s6p)^1P_1^0 || er || (6s6s)^1S_0^0 \rangle, \quad (\text{C2})$$

while the upper one is no longer

$$\mathcal{D}_u = -\langle (6sns)^1S_0^0 || er || (6s6p)^1P_1^0 \rangle,$$

but becomes

$$\mathbb{D}_u = -\langle (6sns)^3S_1 || er || (6s6p)^3P_1^0 \rangle, \quad (\text{C3})$$

if $|(6s6p)^3S_1\rangle$ is used. Here there is no singlet-triplet state mixing for the considered Rydberg states with $F = I+1$ as shown around Eq. (B5), so we do not use the superscript “0” for the Rydberg state $|r\rangle$. To compare \mathcal{D}_u and \mathbb{D}_u ,

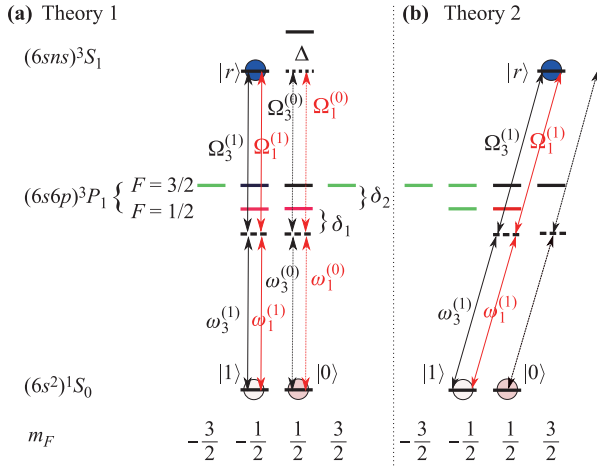


Fig. S1 Rydberg excitation of $|1\rangle$ with Theory 1 in (a), and with Theory 2 in (b). Both the $|0\rangle$ and $|1\rangle$ states of the qubit are excited. In (a), the four Rabi frequencies for exciting the qubit state $|0\rangle$ is indicated, where the red arrows indicate the transition via the $F = 3/2$ sublevel of the intermediate state, while the black arrows are for transitions via the $F = 1/2$ sublevel of the intermediate state. In both (a) and (b), the four Rabi frequencies $\omega_3^{(1)}$, $\omega_1^{(1)}$, $\Omega_3^{(1)}$, and $\Omega_1^{(1)}$ are indicated for exciting the transition from $|1\rangle$ to $|r\rangle$.

we use angular coupling rules to further reduce the radial couplings to

$$\begin{aligned} \mathcal{D}_u &= -\sqrt{3} \begin{Bmatrix} 0 & 1 & 1 \\ 1 & 0 & 0 \end{Bmatrix} \langle (6sns)S || er || (6s6p)P \rangle \\ &= -\langle (6sns)S || er || (6s6p)P \rangle, \\ \mathbb{D}_u &= \sqrt{3} \begin{Bmatrix} 0 & 1 & 1 \\ 1 & 1 & 1 \end{Bmatrix} \langle (6sns)S || er || (6s6p)P \rangle \\ &= -\frac{1}{\sqrt{3}} \langle (6sns)S || er || (6s6p)P \rangle, \end{aligned} \quad (C4)$$

where $\{\dots\}$ is a 6-j symbol and the integration $\langle (6sns)S || er || (6s6p)P \rangle$ is about $-0.0046ea_0$ for $n = 70$ [131] and, thus, $\mathbb{D}_u \approx -1.5 \times 10^{-3}ea_0$.

We then examine the dipole matrix element $\langle (6s6p)^1P_1 || er || (6s^2)^1S_0 \rangle$ for the lower transition $(6s^2)^1S_0 \rightarrow (6s6p)^1P_1$ which has a linewidth $\Gamma = 2\pi \times 29$ MHz [27, 28]. As can be verified [132] by using the Weisskopf–Wigner approximation, the dipole matrix element can be estimated by the following relation [see Eq. (11.33) of Ref. [132]]

$$\Gamma = \frac{\omega_0^3}{\pi\epsilon_0\hbar c^3} |\langle (6s6p)^1P_1 || er || (6s^2)^1S_0 \rangle|^2, \quad (C5)$$

where ϵ_0 is the free-space dielectric permittivity, c is the light speed in vacuum, \hbar is the Planck constant, and $\omega_0/(2\pi) \approx 7.5 \times 10^{14}$ Hz is the transition frequency, which lead to $|\langle (6s6p)^1P_1 || er || (6s^2)^1S_0 \rangle| = 1.38ea_0$. Note that the above estimate has not taken into account of the singlet-triplet mixing as shown in Eq. (A1). In other words, the actual coupling matrix element should include

the factor a in Eq. (A1). However, a is near 1 and, hence, we have $|\langle (6s6p)^1P_1^0 || er || (6s^2)^1S_0 \rangle| = 1.38ea_0$.

The dipole matrix element for the upper transition can be approximated by the semiclassical analytical formulas [104] which have been tested in Ref. [133]. This method is applicable here since the Rydberg state we consider is relatively high, and we can safely assume that the Rydberg electron is far away from the core formed by the nuclear spin and the other electrons in the atom. We have $|\langle (6s70s)S || er || (6s6p)P \rangle| = 0.0046ea_0$ with the estimate in Ref. [131]. However, there is a singlet-triplet state mixing in the Rydberg state, which should be considered if either $|\lambda_+\rangle$ or $|\lambda_-\rangle$ of Eq. (B6) is used as $|r\rangle$.

The above data show that the choice of $(6s6p)^3P_1$ as the intermediate state is more favorable because of Eq. (A1), where $(6s6p)^3P_1$ mainly has the $(6s6p)^3P_1^0$ component and thus can be easily excited to the $(6sns)^3S_1$ state with a dipole matrix element $a\mathbb{D}_u \approx \mathbb{D}_u$. Because of the large transition dipole matrix element between the ground state and the $(6s6p)^1P_1^0$ component in $(6s6p)^3P_1$, the lower transition still has a sizable dipole matrix element $b\mathcal{D}_l$.

D Rabi frequencies in Theory 1

Here, we study Rabi frequencies by choosing the pure triplet Rydberg state as $|r\rangle$ for brevity; data with $|\lambda_+\rangle$ as $|r\rangle$ can be obtained by slightly modifying the results. The laser fields are linearly polarized along the quantization axis for Theory 1. The two qubit states $|0\rangle$ and $|1\rangle$ are both excited to Rydberg states, shown in Fig. S1(a). The used Rydberg state is then $|r\rangle = |(6sns)^3S_1, F = 3/2, m_F = -1/2\rangle$ that can be excited from $|1\rangle \equiv |^1S_0, m_I = -1/2\rangle$. From the ground state to the intermediate state, the $(6s6p)^3P_1^0$ component in $(6s6p)^3P_1$ is not coupled because the transition between triplet and singlet states is spin forbidden. But the $(6s6p)^1P_1^0$ component in $(6s6p)^3P_1$ can be coupled. For the upper transition to the Rydberg state $(6sns)^3S_1$, only the $(6s6p)^3P_1^0$ component in $(6s6p)^3P_1$ is coupled. In essence, the transition is like

$$\begin{aligned} |1\rangle &\rightarrow |(6s6p)^1P_1^0, F = \frac{1(3)}{2}, m_F = -\frac{1}{2}\rangle \text{ [in } (6s6p)^3P_1] \\ |(6s6p)^3P_1^0, F = \frac{1(3)}{2}, m_F = -\frac{1}{2}\rangle &\text{ [in } (6s6p)^3P_1] \rightarrow |r\rangle, \end{aligned} \quad (D1)$$

for $|1\rangle$, and similarly for $|0\rangle$ because the two qubit states are symmetrical to each other. In other words, their transitions to Rydberg states are characterized with similar dipole matrix elements and transition selection rules. To show this, one can calculate the four one-photon Rabi frequencies for the transition from $|1\rangle$ to $|r\rangle$,

$$\begin{aligned} \omega_3^{(1)} &= \mathcal{E}_l \mathcal{D}_l C_3^{(1)}, \\ \omega_1^{(1)} &= \mathcal{E}_l \mathcal{D}_l C_1^{(1)}, \\ \Omega_3^{(1)} &= \mathcal{E}_u \mathbb{D}_u C_3^{(1)'}, \end{aligned}$$

$$\Omega_1^{(1)} = \mathcal{E}_u \mathbb{D}_u C_1^{(1)'}, \quad (\text{D2})$$

where the dipole matrix elements are given by Eqs. (C2) and (C3), and the coefficients $C_3^{(1)}$, $C_1^{(1)}$, $C_3^{(1)'}$, and $C_1^{(1)'}$ are determined by the dipole selection rules and the Wigner-Eckart theorem,

$$\begin{aligned} C_3^{(1)} &= -\sqrt{6} \left\{ \begin{matrix} 1 & 0 & 1 \\ \frac{1}{2} & \frac{3}{2} & \frac{1}{2} \end{matrix} \right\} \mathbb{C}_{\frac{1}{2}0\frac{1}{2}}^{\frac{1}{2}1\frac{3}{2}} \\ &= -\sqrt{6} \cdot (-\sqrt{1/6}) \cdot \sqrt{2/3}, \\ C_1^{(1)} &= -\sqrt{6} \left\{ \begin{matrix} 1 & 0 & 1 \\ \frac{1}{2} & \frac{1}{2} & \frac{1}{2} \end{matrix} \right\} \mathbb{C}_{\frac{1}{2}0\frac{1}{2}}^{\frac{1}{2}1\frac{1}{2}} \\ &= -\sqrt{6} \cdot \sqrt{1/6} \cdot (-\sqrt{1/3}), \\ C_3^{(1)'} &= 2\sqrt{3} \left\{ \begin{matrix} 1 & 1 & 1 \\ \frac{3}{2} & \frac{3}{2} & \frac{1}{2} \end{matrix} \right\} \mathbb{C}_{\frac{1}{2}0\frac{1}{2}}^{\frac{3}{2}1\frac{3}{2}} \\ &= 2\sqrt{3} \cdot (\sqrt{10}/12) \cdot (-\sqrt{1/15}), \\ C_1^{(1)'} &= -\sqrt{6} \left\{ \begin{matrix} 1 & 1 & 1 \\ \frac{1}{2} & \frac{3}{2} & \frac{1}{2} \end{matrix} \right\} \mathbb{C}_{\frac{1}{2}0\frac{1}{2}}^{\frac{1}{2}1\frac{3}{2}} \\ &= -\sqrt{6} \cdot (-1/6) \cdot (\sqrt{2/3}), \end{aligned} \quad (\text{D3})$$

where $\mathbb{C}[\dots]$ denotes a Clebsch-Gordan coefficient and $\{\dots\}$ is a 6-j symbol. From the above results we can derive by adiabatic elimination [105] that the effective two-photon Rabi frequency between $|1\rangle$ and $|(6sns)^3S_1, F=3/2, m_F=-1/2\rangle$ is

$$\begin{aligned} \Omega_{1r} &= -\frac{\omega_1^{(1)}\Omega_1^{(1)}}{2\delta_1} - \frac{\omega_3^{(1)}\Omega_3^{(1)}}{2(\delta_1 + \delta_2)} \\ &= -\frac{\mathcal{E}_l\mathcal{E}_u\mathcal{D}_l\mathbb{D}_u}{3\sqrt{3}} \left[\frac{1}{2\delta_1} - \frac{1}{2(\delta_1 + \delta_2)} \right], \end{aligned} \quad (\text{D4})$$

where δ_1 is given by the frequency of the lower laser field minus the frequency of the atomic transition $|1\rangle \leftrightarrow |(6sns)^3P_1, F=1/2, m_F=-1/2\rangle$, and $-\delta_2$ is the hyperfine gap between the $F=1/2$ and $F=3/2$ levels. We have $-\delta_2 = 2\pi \times 5.94$ GHz according to [88, 93]. By deriving the effective Rabi frequency, there is some Stark shift which we assume to be compensated by calibrating the detunings, field amplitudes, and if necessary, extra highly off-resonant dressing fields [17, 106]. In numerical simulations these shifts are included, shown in Eqs. (10) and (11).

To verify that the transitions from $|0\rangle$ to the Rydberg state has similar property as that from $|1\rangle$, we study the four coefficients related with the Rabi frequencies for the transition from $|0\rangle$,

$$\begin{aligned} C_3^{(0)} &= -\sqrt{6} \left\{ \begin{matrix} 1 & 0 & 1 \\ \frac{1}{2} & \frac{3}{2} & \frac{1}{2} \end{matrix} \right\} \mathbb{C}_{\frac{1}{2}0\frac{1}{2}}^{\frac{1}{2}1\frac{3}{2}} \\ &= -\sqrt{6} \cdot (-\sqrt{1/6}) \cdot \sqrt{2/3}, \\ C_1^{(0)} &= -\sqrt{6} \left\{ \begin{matrix} 1 & 0 & 1 \\ \frac{1}{2} & \frac{1}{2} & \frac{1}{2} \end{matrix} \right\} \mathbb{C}_{\frac{1}{2}0\frac{1}{2}}^{\frac{1}{2}1\frac{1}{2}} \end{aligned}$$

$$= -\sqrt{6} \cdot \sqrt{1/6} \cdot \sqrt{1/3},$$

$$\begin{aligned} C_3^{(0)'} &= 2\sqrt{3} \left\{ \begin{matrix} 1 & 1 & 1 \\ \frac{3}{2} & \frac{3}{2} & \frac{1}{2} \end{matrix} \right\} \mathbb{C}_{\frac{1}{2}0\frac{1}{2}}^{\frac{3}{2}1\frac{3}{2}} \\ &= 2\sqrt{3} \cdot (\sqrt{10}/12) \cdot \sqrt{1/15}, \\ C_1^{(0)'} &= -\sqrt{6} \left\{ \begin{matrix} 1 & 1 & 1 \\ \frac{1}{2} & \frac{3}{2} & \frac{1}{2} \end{matrix} \right\} \mathbb{C}_{\frac{1}{2}0\frac{1}{2}}^{\frac{1}{2}1\frac{3}{2}} \\ &= -\sqrt{6} \cdot (-1/6) \cdot (\sqrt{2/3}), \end{aligned} \quad (\text{D5})$$

from which one can derive the effective Rabi frequency from $|0\rangle$ to the Rydberg state $|(6sns)^3S_1, F=3/2, m_F=1/2\rangle$ as

$$\begin{aligned} \Omega_{0r} &= -\frac{\omega_1^{(0)}\Omega_1^{(0)}}{2\delta_1} - \frac{\omega_3^{(0)}\Omega_3^{(0)}}{2(\delta_1 + \delta_2)} \\ &= \frac{\mathcal{E}_l\mathcal{E}_u\mathcal{D}_l\mathbb{D}_u}{3\sqrt{3}} \left[\frac{1}{2\delta_1} - \frac{1}{2(\delta_1 + \delta_2)} \right]. \end{aligned} \quad (\text{D6})$$

In order to have a larger Rabi frequency, a positive δ_1 that is smaller than $-\delta_2$ is preferred. The transition from the ground state to the $(6s6p)^3P_1$ state needs light of wavelength of about 556 nm [88, 93], and its transition to the Rydberg state with $n=70$ needs radiation of wavelength 308.4 nm (According to Ref. [103] the energy of $6s70s$ state is 50417.7 cm^{-1} , while the energy of $(6s6p)^3P_1$ state is 17992.01 cm^{-1} [90]). Although the 308 nm UV laser appeared less frequently in the literature, a laser system with wavelength tunable in the range 304–309 nm was used in the experiments [95] to excite Rydberg states of a strontium ion (see also Refs. [96, 97] where similar lasers were used for Rydberg excitations of ions). Such UV lasers were usually prepared by frequency doubling via second-harmonic generation (see the supplementary information of Ref. [97]) where similar powers can be obtained for similar frequencies, and, thus, we analyze achievable laser powers by the more frequently used 319 nm lasers.

The lower transition has a dipole matrix element on the order of ea_0 as shown below Eq. (C5). Such a magnitude is of similar magnitude to that of the lower transition in exciting a Rydberg state of rubidium or cesium where Rabi frequencies up to $2\pi \times 300$ MHz could be achieved [14], and, hence, we assume $\omega_1^{(1)}/(2\pi) = 300$ MHz. However, the dipole matrix element for the upper transition is tiny, and then the Rabi frequency for the upper transition is mainly determined by the achievable strength of the electric field \mathcal{E}_u in the UV lasers. In Ref. [122], Rydberg excitation from the $(5s5p)^3P_1$ of strontium was achieved with ultraviolet light at 319 nm with a power 34 mW. In Ref. [97], a 306 nm laser with power 60 mW focused to a waist of 8 μm was used for preparing Rydberg ions (Ref. [97] indicates that their laser power can in principle be increased by two orders of magnitude). In Ref. [65], Rydberg excitation of the $84p$ state of cesium was achieved by a 319 nm light with a laser

power 300 mW. Thus, we assume a laser power 300mW in our estimate. To avoid error in the laser Rabi frequencies from position fluctuation of atoms, we assume a beam waist 10 μm as in the experiment in Ref. [65]. Then $\mathcal{E}_u = \sqrt{2I/(c\epsilon_0)} \approx 2.5 \times 10^6$ V/m, where $I \approx 300$ mW/(100 π μm^2), c is the speed of light in vacuum, and ϵ_0 is the free space permittivity. This is a strong field but it is experimentally feasible; see, e.g., page 2 of Ref. [65] that shows a similarly huge UV laser field with intensity 6×10^8 W/m² at the atoms. With $|\mathbb{D}_u| \approx 0.0046e a_0/3$ for $n = 70$ [131] [here the factor 1/3 is from Eq. (C4)], we have $\Omega_1^{(1)} = \mathcal{E}_u \mathcal{D}_u C_1^{(1)'}/\hbar \approx 2\pi \times 103$ MHz. From Eq. (D5) we have $\omega_1^{(1)} \Omega_1^{(1)} = -\omega_1^{(0)} \Omega_1^{(0)}$, and, thus, setting $\delta_1 = -(\delta_1 + \delta_2)$ can maximize the effective Rabi frequency, which requires $\delta_1 = -\delta_2/2 = 2\pi \times 2.97$ GHz. The above estimate shows that reaching a Rydberg Rabi frequency $|\Omega_{1r}|/(2\pi) = 300 \cdot 103/(2970) \approx 10.4$ MHz is possible. However, according to Eq. (A1), Appendix B, and Appendix C, the actual Rabi frequency for the lower transition shall be multiplied by a factor of b , and, thus, the final achievable Rabi frequency is

$$|\Omega_{1r}|/(2\pi) = (300b) \cdot 103/2970 \approx 1.4 \text{ MHz.} \tag{D7}$$

Note that a large ratio between $\delta_{1(2)}$ and the single-photon Rabi frequencies is required in deriving the effective two-photon Rabi frequency. In the above case, the ratios are $2970/(300b) \approx 74$ and $2970/103 \approx 29$ for the lower and upper transitions, respectively. This can lead to high-fidelity control over the Rydberg excitations.

Comparing Eq. (D6) and Eq. (D4) shows that the state $|0\rangle$ is excited to Rydberg states with a Rabi frequency $-\Omega_{1r}$. Note that the magnetic field can induce some energy difference between the intermediate states for exciting $|0\rangle$ and $|1\rangle$. But compared to the GHz-scale $\delta_{1(2)}$, they are negligible when the applied magnetic field is on the order of 1 G that does not change the picture described above. In a magnetic field the splitting between $|0\rangle$ and $|1\rangle$ is $g_I \mu_n B \approx 2\pi \times 1.5$ kHz with $B = 3.9$ G and $\mu_n = 0.4919 \mu_N$ for ^{171}Yb [83]. The $m_F = \pm 1/2$ levels of the Rydberg states have a Zeeman shift $g_J \mu_B B$. In this work we assume $g_J = g_L = 1$ although it is 0.87 for the choice of $|r\rangle$ analyzed below Eq. (B8).

E Rabi frequencies in Theory 2

In Theory 2, circularly polarized laser fields are used, as shown in Fig. S1(b). Because the 3S_1 state does not have a $m_F = 5/2$ state, the qubit state $|0\rangle$ cannot be excited to the Rydberg state, and only $|1\rangle$ can go to the Rydberg state. Both the lower and upper fields are right-hand polarized, with field amplitudes \mathcal{E}_l and \mathcal{E}_u , respectively. We calculate the four one-photon Rabi frequencies for the

transition from $|1\rangle$ to $|r\rangle$,

$$\begin{aligned} \omega_3^{(1)} &= \mathcal{E}_l \mathcal{D}_l C_3^{(1)}, \\ \omega_1^{(1)} &= \mathcal{E}_l \mathcal{D}_l C_1^{(1)}, \\ \Omega_3^{(1)} &= \mathcal{E}_u \mathbb{D}_u C_3^{(1)'}, \\ \Omega_1^{(1)} &= \mathcal{E}_u \mathbb{D}_u C_1^{(1)'}, \end{aligned} \tag{E1}$$

where the dipole matrix elements are given by Eqs. (C2) and (C3), and the coefficients $C_3^{(1)}$, $C_1^{(1)}$, $C_3^{(1)'}$, and $C_1^{(1)'}$ are determined by the dipole selection rules and the Wigner-Eckart theorem,

$$\begin{aligned} C_3^{(1)} &= -\sqrt{6} \left\{ \begin{matrix} 1 & 0 & 1 \\ \frac{1}{2} & \frac{3}{2} & \frac{1}{2} \end{matrix} \right\} C_{\frac{1}{2} \frac{1}{2} \frac{3}{2}}^{\frac{1}{2} 1 \frac{3}{2}} \\ &= -\sqrt{6} \cdot (-\sqrt{1/6}) \cdot \sqrt{1/3}, \\ C_1^{(1)} &= -\sqrt{6} \left\{ \begin{matrix} 1 & 0 & 1 \\ \frac{1}{2} & \frac{1}{2} & \frac{1}{2} \end{matrix} \right\} C_{\frac{1}{2} \frac{1}{2} \frac{1}{2}}^{\frac{1}{2} 1 \frac{1}{2}} \\ &= -\sqrt{6} \cdot \sqrt{1/6} \cdot (-\sqrt{2/3}), \\ C_3^{(1)'} &= 2\sqrt{3} \left\{ \begin{matrix} 1 & 1 & 1 \\ \frac{3}{2} & \frac{3}{2} & \frac{1}{2} \end{matrix} \right\} C_{\frac{1}{2} \frac{1}{2} \frac{3}{2}}^{\frac{3}{2} 1 \frac{3}{2}} \\ &= 2\sqrt{3} \cdot (\sqrt{10/12}) \cdot (-\sqrt{2/5}), \\ C_1^{(1)'} &= -\sqrt{6} \left\{ \begin{matrix} 1 & 1 & 1 \\ \frac{1}{2} & \frac{3}{2} & \frac{1}{2} \end{matrix} \right\} C_{\frac{1}{2} \frac{1}{2} \frac{3}{2}}^{\frac{1}{2} 1 \frac{3}{2}} \\ &= -\sqrt{6} \cdot (-1/6) \cdot (1). \end{aligned} \tag{E2}$$

Comparing Eq. (D5) and Eq. (E2) shows that the Rabi frequencies $(\omega_3^{(1)}, \omega_1^{(1)}, \Omega_3^{(1)}, \Omega_1^{(1)})$ here are $(1/\sqrt{2}, \sqrt{2}, \sqrt{6}, \sqrt{6}/2)$ times those in Eq. (D2). From the above results we can derive by adiabatic elimination [105] that the effective two-photon Rabi frequency between $|1\rangle$ and $|(6sns)^3S_1, F = 3/2, m_F = -1/2\rangle$ is

$$\begin{aligned} \Omega_{1r} &= -\frac{\omega_1^{(1)} \Omega_1^{(1)}}{2\delta_1} - \frac{\omega_3^{(1)} \Omega_3^{(1)}}{2(\delta_1 + \delta_2)} \\ &= -\frac{\mathcal{E}_l \mathcal{E}_u \mathcal{D}_l \mathbb{D}_u}{3} \left[\frac{1}{2\delta_1} - \frac{1}{2(\delta_1 + \delta_2)} \right], \end{aligned} \tag{E3}$$

which is $\sqrt{3}$ times Eq. (D4) mainly because the angular factor is larger than that in deriving Eq. (D4) because of different polarizations in the laser fields. With a similar analysis leading to Eq. (D7), we estimate that the Rydberg Rabi frequency for $|1\rangle \rightarrow |r\rangle$ can reach $2\pi \times 2.4$ MHz. For the transition from $|0\rangle$ to $|(6s6p)^3P_1, F = 3/2, m_F = 3/2\rangle$ with a detuning $\delta_1 + \delta_2 \approx 2\pi \times (-2.97)$ GHz, the Rabi frequency is

$$\omega_3^{(0)} = \mathcal{E}_l \mathcal{D}_l C_3^{(0)}, \tag{E4}$$

with

$$C_3^{(0)} = -\sqrt{6} \left\{ \begin{matrix} 1 & 0 & 1 \\ \frac{1}{2} & \frac{3}{2} & \frac{1}{2} \end{matrix} \right\} C_{\frac{1}{2} \frac{1}{2} \frac{3}{2}}^{\frac{1}{2} 1 \frac{3}{2}}$$

$$= -\sqrt{6} \cdot (-\sqrt{1/6}) \cdot 1,$$

which leads to $300\sqrt{3/2}\beta \approx 2\pi \times 49$ MHz according to the estimate above Eq. (D7). This means that the leakage to the intermediate state is on the order of $(40/2970)^2/2 \approx 1.4 \times 10^{-4}$ that is negligible compared to the decay errors. On the other hand, the tiny population on the 3P_1 state also leads to decay from it. However, this is negligible. For a π pulse on the qubit state $|1\rangle$, the time for the atom initialized in the qubit state $|0\rangle$ to stay at the 3P_1 level is about $(49/2970)^2 \cdot \pi/|2\Omega_{1r}| \approx 0.028$ ns, which leads to an extra decay error 3.5×10^{-5} from 3P_1 by taking a lifetime 800 ns for it [90]. Such an error is orders of magnitude smaller than that from the Rydberg-state decay and, hence, can be neglected.

F Data with ^{87}Sr

The spin-orbit coupling in ^{87}Sr leads to

$$\begin{aligned} |(5s5p)^1P_1\rangle &= a|(5s5p)^1P_1^0\rangle - b|(5s5p)^3P_1^0\rangle, \\ |(5s5p)^3P_1\rangle &= b|(5s5p)^1P_1^0\rangle + a|(5s5p)^3P_1^0\rangle, \end{aligned} \quad (\text{F1})$$

where (a, b) depend on the strength of the spin-orbit coupling in the specific AEL element. We have $(a, b) = (0.9996, -0.0286)$ for strontium according to Ref. [91]. Compared to Eq. (A1) for ytterbium, the mixing characterized by b is about five times weaker here, which leads to a long lifetime 21.5 μs [134] of strontium $|(5s5p)^3P_1\rangle$ (the lifetime of ytterbium $|(5s5p)^3P_1\rangle$ is less than 1 μs).

For the dipole matrix element $\langle(5s5p)^1P_1||er||5s^2)^1S_0\rangle$ with a linewidth of $\Gamma = 2\pi \times 32$ MHz [120, 135] and transition frequency $\omega_0/(2\pi) \approx 6.5 \times 10^{14}$ Hz, we use

$$\Gamma = \frac{\omega_0^3}{\pi\epsilon_0\hbar c^3} |\langle(5s5p)^1P_1||er||5s^2)^1S_0\rangle|^2, \quad (\text{F2})$$

to estimate $|\langle(5s5p)^1P_1||er||5s^2)^1S_0\rangle| = 1.80ea_0$. This means that if we choose $|(5s5p)^3P_1\rangle$ as the intermediate state, the dipole matrix element between it and the ground state is only $|1.80ea_0 \cdot b| \approx 0.05ea_0$. Compared to the case with ytterbium where $|\langle(6s6p)^3P_1||er||6s^2)^1S_0\rangle| = 0.18ea_0$, Rydberg excitation via the $|(5s5p)^3P_1\rangle$ state of strontium is much more difficult.

A more useful choice for the intermediate state is $|(5s6p)^1P_1\rangle$ with a linewidth $\Gamma = 2\pi \times 0.3$ MHz and a 293 nm excitation wavelength (which can be prepared via second-harmonic generation [95–97]). With a method similar to Eq. (F2), we find that $|\langle(5s6p)^1P_1||er||5s^2)^1S_0\rangle| = 0.088ea_0$. This means that the $|(5s6p)^1P_1\rangle$ state is indeed a useful choice. But the coupling between the intermediate and Rydberg 3S_1 states is spin forbidden, so we consider the 1S_0 Rydberg state. However, the 1S_0 Rydberg state is strongly mixed with the 3S_1 Rydberg state [114]. As studied in Ref. [114], the mixing leads to two split states with a GHz-scale energy separation, so it is possible to use the hyperfine-mixed state as $|r\rangle$. Importantly,

because of the triplet component in $|r\rangle$ there can also be a strong Zeeman shift when a B -field on the order of 1 G is applied.

With $|(5s6p)^1P_1\rangle$ as the intermediate state, the dipole matrix element \mathcal{D}_u for the upper transition here is of similar magnitude to that for the upper transition of ytterbium in Fig. S1. This is because the final reduced matrix elements are both expressed as $\langle ns||er||6p\rangle$. According to Eq. (C4), however, $|\mathcal{D}_u|$ is $\sqrt{3}$ times larger than $|\mathbb{D}_u|$, which means that the matrix element between the $|(5s6p)^1P_1\rangle$ and $|(5s70s)^1S_0\rangle$ states of ^{87}Sr is $\sqrt{3}$ times larger than that of Fig. S1. Then, the achievable Rydberg Rabi frequency for $|1\rangle \rightarrow |70^1S_0\rangle$ is $\sqrt{3} \cdot 0.088ea_0/(0.18ea_0) \approx 0.8$ times those in Eqs. (D7) and (E3) for Theory 1 and Theory 2, respectively. Of course, such an estimate assumes the same hyperfine gap $|\delta_2|$ and detuning δ_1 as in Fig. S1. In practice, this is not crucial since we can choose appropriate δ_1 so as to have a large enough Rydberg Rabi frequency described above; the negative effect is that with smaller δ_1 there can be more scattering from the intermediate state.

References

1. M. A. Nielsen and I. L. Chuang, *Quantum Computation and Quantum Information*, Cambridge University Press, Cambridge, 2000
2. T. D. Ladd, F. Jelezko, R. Laflamme, Y. Nakamura, C. Monroe, and J. L. O'Brien, Quantum computers, *Nature* (London) 464, 45 (2010)
3. R. Blatt and D. Wineland, Entangled states of trapped atomic ions, *Nature* 453, 1008 (2008)
4. J. Q. You and F. Nori, Superconducting circuits and quantum information, *Phys. Today* 58, 42 (2005)
5. J. Q. You and F. Nori, Atomic physics and quantum optics using superconducting circuits, *Nature* 474, 589 (2011)
6. D. D. Awschalom, L. C. Bassett, A. S. Dzurak, E. L. Hu, and J. R. Petta, Quantum Spintronics: Engineering and manipulating atom-like spins in semiconductors, *Science* 339, 1174 (2013)
7. M. H. Devoret and R. J. Schoelkopf, Superconducting circuits for quantum information: An outlook, *Science* 339, 1169 (2013)
8. D. Jaksch, J. I. Cirac, P. Zoller, S. L. Rolston, R. Côté, and M. D. Lukin, Fast quantum gates for neutral atoms, *Phys. Rev. Lett.* 85, 2208 (2000)
9. M. D. Lukin, M. Fleischhauer, R. Cote, L. M. Duan, D. Jaksch, J. I. Cirac, and P. Zoller, Dipole blockade and quantum information processing in mesoscopic atomic ensembles, *Phys. Rev. Lett.* 87, 037901 (2001)
10. M. Saffman, T. G. Walker, and K. Mølmer, Quantum information with Rydberg atoms, *Rev. Mod. Phys.* 82, 2313 (2010)
11. M. Saffman, Quantum computing with atomic qubits and Rydberg interactions: Progress and challenges, *J. Phys. B* 49, 202001 (2016)

12. D. S. Weiss and M. Saffman, Quantum computing with neutral atoms, *Phys. Today* 70, 44 (2017)
13. C. S. Adams, J. D. Pritchard, and J. P. Shaffer, Rydberg atom quantum technologies, *J. Phys. B: At. Mol. Opt. Phys.* 53, 012002 (2020)
14. T. Wilk, A. Gaëtan, C. Evellin, J. Wolters, Y. Miroshnychenko, P. Grangier, and A. Browaeys, Entanglement of two individual neutral atoms using Rydberg blockade, *Phys. Rev. Lett.* 104, 010502 (2010)
15. L. Isenhower, E. Urban, X. L. Zhang, A. T. Gill, T. Henage, T. A. Johnson, T. G. Walker, and M. Saffman, Demonstration of a neutral atom controlled-NOT quantum gate, *Phys. Rev. Lett.* 104, 010503 (2010)
16. X. L. Zhang, L. Isenhower, A. T. Gill, T. G. Walker, and M. Saffman, Deterministic entanglement of two neutral atoms via Rydberg blockade, *Phys. Rev. A* 82, 030306(R) (2010)
17. K. M. Maller, M. T. Lichtman, T. Xia, Y. Sun, M. J. Piotrowicz, A. W. Carr, L. Isenhower, and M. Saffman, Rydberg-blockade controlled-NOT gate and entanglement in a two-dimensional array of neutral-atom qubits, *Phys. Rev. A* 92, 022336 (2015)
18. Y.-Y. Jau, A. M. Hankin, T. Keating, I. H. Deutsch, and G. W. Biedermann, Entangling atomic spins with a Rydberg-dressed spin-flip blockade, *Nat. Phys.* 12, 71(2016)
19. Y. Zeng, P. Xu, X. He, Y. Liu, M. Liu, J. Wang, D. J. Papoular, G. V. Shlyapnikov, and M. Zhan, Entangling two individual atoms of different isotopes via Rydberg blockade, *Phys. Rev. Lett.* 119, 160502 (2017)
20. H. Levine, A. Keesling, A. Omran, H. Bernien, S. Schwartz, A. S. Zibrov, M. Endres, M. Greiner, V. Vuletić, and M. D. Lukin, High-fidelity control and entanglement of Rydberg atom qubits, *Phys. Rev. Lett.* 121, 123603 (2018)
21. C. J. Picken, R. Legaie, K. McDonnell, and J. D. Pritchard, Entanglement of neutral-atom qubits with long ground-Rydberg coherence times, *Quant. Sci. Technol.* 4, 015011 (2019)
22. H. Levine, A. Keesling, G. Semeghini, A. Omran, T. T. Wang, S. Ebadi, H. Bernien, M. Greiner, V. Vuletić, H. Pichler, and M. D. Lukin, Parallel implementation of high-fidelity multi-qubit gates with neutral atoms, *Phys. Rev. Lett.* 123, 170503 (2019)
23. T. M. Graham, M. Kwon, B. Grinkemeyer, Z. Marra, X. Jiang, M. T. Lichtman, Y. Sun, M. Ebert, and M. Saffman, Rydberg mediated entanglement in a two-dimensional neutral atom qubit array, *Phys. Rev. Lett.* 123, 230501 (2019)
24. H. Jo, Y. Song, M. Kim, and J. Ahn, Rydberg atom entanglements in the weak coupling regime, *Phys. Rev. Lett.* 124, 33603 (2019)
25. I. S. Madjarov, J. P. Covey, A. L. Shaw, J. Choi, A. Kale, A. Cooper, H. Pichler, V. Schkolnik, J. R. Williams, and M. Endres, High-fidelity entanglement and detection of alkaline-earth Rydberg atoms, *Nat. Phys.* 16, 857 (2020)
26. D. Crow, R. Joynt, and M. Saffman, Improved error thresholds for measurement-free error correction, *Phys. Rev. Lett.* 117, 130503 (2016)
27. R. Yamamoto, J. Kobayashi, T. Kuno, K. Kato, and Y. Takahashi, An ytterbium quantum gas microscope with narrow-line laser cooling, *New J. Phys.* 18, 023016 (2016)
28. S. Saskin, J. T. Wilson, B. Grinkemeyer, and J. D. Thompson, Narrow-line cooling and imaging of Ytterbium atoms in an optical tweezer array, *Phys. Rev. Lett.* 122, 143002 (2019)
29. A. Cooper, J. P. Covey, I. S. Madjarov, S. G. Porsev, M. S. Safronova, and M. Endres, Alkaline-earth atoms in optical tweezers, *Phys. Rev. X* 8, 41055 (2018)
30. J. P. Covey, I. S. Madjarov, A. Cooper, and M. Endres, 2000-times repeated imaging of strontium atoms in clock-magic tweezer arrays, *Phys. Rev. Lett.* 122, 173201 (2019)
31. M. A. Norcia, A. W. Young, and A. M. Kaufman, Microscopic control and detection of ultracold strontium in optical-tweezer arrays, *Phys. Rev. X* 8, 041054 (2018)
32. I. Reichenbach and I. H. Deutsch, Sideband cooling while preserving coherences in the nuclear spin state in group-II-like atoms, *Phys. Rev. Lett.* 99, 123001 (2007)
33. J. Wilson, S. Saskin, Y. Meng, S. Ma, R. Dilip, A. Burgers, and J. Thompson, Trapped arrays of alkaline earth Rydberg atoms in optical tweezers, arXiv: 1912.08754 [quant-ph] (2019)
34. X.-F. Shi, Rydberg quantum gates free from blockade error, *Phys. Rev. Appl.* 7, 064017 (2017)
35. K. Bergmann, H. Theuer, and B. W. Shore, Coherent population transfer among quantum states of atoms and molecules, *Rev. Mod. Phys.* 70, 1003 (1998)
36. P. Král, I. Thanopoulos, and M. Shapiro, Coherently controlled adiabatic passage, *Rev. Mod. Phys.* 79, 53 (2007)
37. N. V. Vitanov, A. A. Rangelov, B. W. Shore, and K. Bergmann, Stimulated Raman adiabatic passage in physics, chemistry, and beyond, *Rev. Mod. Phys.* 89, 015006 (2017)
38. D. Møller, L. B. Madsen, and K. Mølmer, Quantum gates and multiparticle entanglement by Rydberg excitation blockade and adiabatic passage, *Phys. Rev. Lett.* 100, 170504 (2008)
39. M. Müller, I. Lesanovsky, H. Weimer, H. P. Büchler, and P. Zoller, Mesoscopic Rydberg gate based on electromagnetically induced transparency, *Phys. Rev. Lett.* 102, 170502 (2009)
40. M. H. Goerz, T. Calarco, and C. P. Koch, The quantum-speed limit of optimal controlled phase gates for trapped neutral atoms, *J. Phys. B* 44 (2011)
41. I. I. Beterov, D. B. Tretyakov, V. M. Entin, E. A. Yakshina, I. I. Ryabtsev, C. MacCormick, and S. Bergamini, Deterministic single-atom excitation via adiabatic passage and Rydberg blockade, *Phys. Rev. A* 84, 023413 (2011)
42. M. M. Müller, H. R. Haakh, T. Calarco, C. P. Koch, and C. Henkel, Prospects for fast Rydberg gates on an atom chip, *Quant. Inf. Proc.* 10, 771 (2011)
43. T. Keating, K. Goyal, Y.-Y. Jau, G. W. Biedermann, A. J. Landahl, and I. H. Deutsch, Adiabatic quantum computation with Rydberg-dressed atoms, *Phys. Rev. A* 87, 052314 (2013)

44. D. Petrosyan and K. Mølmer, Stimulated adiabatic-passage in a dissipative ensemble of atoms with strong Rydberg-state interactions, *Phys. Rev. A* 87, 033416 (2013)
45. I. I. Beterov, M. Saffman, E. a. Yakshina, V. P. Zhukov, D. B. Tretyakov, V. M. Entin, I. I. Ryabtsev, C. W. Mansell, C. McCormick, S. Bergamini, and M. P. Fedoruk, Quantum gates in mesoscopic atomic ensembles-based on adiabatic passage and Rydberg blockade, *Phys. Rev. A* 88, 010303(R) (2013)
46. M. M. Müller, M. Murphy, S. Montangero, T. Calarco, P. Grangier, and A. Browaeys, Implementation of an experimentally feasible controlled-phase gate on two blocked Rydberg atoms, *Phys. Rev. A* 89, 032334 (2014)
47. M. H. Goerz, E. J. Halperin, J. M. Aytac, C. P. Koch, and K. B. Whaley, Robustness of high-fidelity Rydberg gates with single-site addressability, *Phys. Rev. A* 90, 032329 (2014)
48. I. I. Beterov, M. Saffman, V. P. Zhukov, D. B. Tretyakov, V. M. Entin, E. A. Yakshina, I. I. Ryabtsev, C. W. Mansell, C. McCormick, S. Bergamini, and M. P. Fedoruk, Coherent control of mesoscopic atomic ensembles for quantum information, *Laser Phys.* 24, 074013 (2014)
49. T. Keating, R. L. Cook, A. M. Hankin, Y.-Y. Jau, G. W. Biedermann, and I. H. Deutsch, Robust quantum logic in neutral atoms via adiabatic Rydberg dressing, *Phys. Rev. A* 91, 012337 (2015)
50. I. I. Beterov, M. Saffman, E. A. Yakshina, D. B. Tretyakov, V. M. Entin, G. N. Hamzina, and I. I. Ryabtsev, Simulated quantum process tomography of quantum gates with Rydberg superatoms, *J. Phys. B* 49, 114007 (2016)
51. L. S. Theis, F. Motzoi, F. K. Wilhelm, and M. Saffman, High-fidelity Rydberg-blockade entangling gate using-shaped, analytic pulses, *Phys. Rev. A* 94, 032306 (2016)
52. H. Wu, X. R. Huang, C. S. Hu, Z. B. Yang, and S. B. Zheng, Rydberg-interaction gates via adiabatic passage and phase control of driving fields, *Phys. Rev. A* 96, 022321 (2017)
53. D. Petrosyan, F. Motzoi, M. Saffman, and K. Mølmer, High-fidelity Rydberg quantum gate via a two-atom dark state, *Phys. Rev. A* 96, 042306 (2017)
54. Y.-H. Kang, Y.-H. Chen, Z.-C. Shi, B.-H. Huang, J. Song, and Y. Xia, Nonadiabatic holonomic quantum computation using Rydberg blockade, *Phys. Rev. A* 97, 042336 (2018)
55. A. Omran, H. Levine, A. Keesling, G. Semeghini, T. T. Wang, S. Ebadi, H. Bernien, A. S. Zibrov, H. Pichler, S. Choi, J. Cui, M. Rossignolo, P. Rembold, S. Montangero, T. Calarco, M. Endres, M. Greiner, V. Vuletić, and M. D. Lukin, Generation and manipulation of Schrödinger cat states in Rydberg atom arrays, *Science* 365, 570 (2019)
56. K.-Y. Liao, X.-H. Lu, Z. Li, and Y.-X. Du, Geometric Rydberg quantum gate with shortcuts to adiabaticity, *Opt. Lett.* 44, 4801 (2019)
57. Y. Sun, P. Xu, P.-X. Chen, and L. Liu, Controlled phase gate protocol for neutral atoms via off-resonant, *Phys. Rev. Appl.* 13, 024059 (2020)
58. X.-F. Shi, Single-site Rydberg addressing in 3D atom arrays for quantum computing with neutral atoms, *J. Phys. B* 53, 054002 (2020)
59. A. Mitra, M. J. Martin, G. W. Biedermann, A. M. Marino, P. M. Poggi, and I. H. Deutsch, Robust Molmer-Sorenson gate for neutral atoms using rapid adiabatic Rydberg dressing, *Phys. Rev. A* 101, 030301(R) (2020)
60. I. I. Beterov, D. B. Tretyakov, V. M. Entin, E. A. Yakshina, I. I. Ryabtsev, M. Saffman, and S. Bergamini, Application of adiabatic passage in Rydberg atomic ensembles for quantum information processing, *J. Phys. B* 53, 182001 (2020)
61. M. Saffman, I. I. Beterov, A. Dalal, E. J. Paez, and B. C. Sanders, Symmetric Rydberg controlled-Z gates with adiabatic pulses control target, *Phys. Rev. A* 101, 62309 (2020)
62. Y.-H. Kang, Z.-C. Shi, J. Song, and Y. Xia, Heralded atomic nonadiabatic holonomic quantum computation with Rydberg blockade, *Phys. Rev. A* 102, 022617 (2020)
63. C.-Y. Guo, L. L. Yan, S. Zhang, S.-L. Su, and W. Li, Optimized geometric quantum computation with mesoscopic ensemble of Rydberg atoms, *Phys. Rev. A* 102, 042607 (2020)
64. M. Khazali and K. Molmer, Fast multiqubit gates by adiabatic evolution in interacting excited-state manifolds of Rydberg atoms and superconducting circuits, *Phys. Rev. X* 10, 21054 (2020)
65. A. M. Hankin, Y.-Y. Jau, L. P. Parazzoli, C. W. Chou, D. J. Armstrong, A. J. Landahl, and G. W. Biedermann, Two-atom Rydberg blockade using direct 6S to nP excitation. *Phys. Rev. A* 89, 033416 (2014)
66. R. C. Teixeira, A. Larrouy, A. Muni, L. Lachaud, J. M. Raimond, S. Gleyzes, and M. Brune, Preparation of long-lived, non-autoionizing circular Rydberg states of strontium, *Phys. Rev. Lett.* 125, 263001 (2020)
67. D. Jaksch, H. J. Briegel, J. I. Cirac, C. W. Gardiner, and P. Zoller, Entanglement of atoms via cold controlled collisions, *Phys. Rev. Lett.* 82, 1975 (1999)
68. T. Calarco, E. A. Hinds, D. Jaksch, J. Schmiedmayer, J. I. Cirac, and P. Zoller, Quantum gates with neutral atoms: Controlling collisional interactions in time dependent traps, *Phys. Rev. A* 61, 022304 (2000)
69. D. Hayes, P. S. Julienne, and I. H. Deutsch, Quantum logic via the exchange blockade in ultracold collisions, *Phys. Rev. Lett.* 98, 070501 (2007)
70. J. P. Covey, A. Sipahigil, S. Szoke, N. Sinclair, M. Endres, and O. Painter, Telecom-band quantum optics with ytterbium atoms and silicon nanophotonics, *Phys. Rev. Appl.* 11, 034044 (2019)
71. A. J. Daley, M. M. Boyd, J. Ye, and P. Zoller, Quantum computing with alkaline-earth-metal atoms, *Phys. Rev. Lett.* 101, 170504 (2008)
72. G. Cappellini, M. Mancini, G. Pagano, P. Lombardi, L. Livi, M. Siciliani de Cumis, P. Cancio, M. Pizzocaro, D. Calonico, F. Levi, C. Sias, J. Catani, M. Inguscio, and L. Fallani, Direct observation of coherent interorbital spin-exchange dynamics, *Phys. Rev. Lett.* 113, 120402 (2014)

73. F. Scazza, C. Hofrichter, M. Höfer, P. C. De Groot, I. Bloch, and S. Fölling, Observation of two-orbital spin-exchange interactions with ultracold $SU(N)$ -symmetric fermions, *Nat. Phys.* 10, 779 (2014)
74. A. M. Kaufman, B. J. Lester, M. Foss-Feig, M. L. Wall, A. M. Rey, and C. A. Regal, Entangling two transportable neutral atoms via local spin exchange, *Nature* 527, 208 (2015)
75. A. V. Gorshkov, A. M. Rey, A. J. Daley, M. M. Boyd, J. Ye, P. Zoller, and M. D. Lukin, Alkaline earth-metal atoms as few-qubit quantum registers, *Phys. Rev. Lett.* 102, 110503 (2009)
76. A. J. Daley, J. Ye, and P. Zoller, State-dependent lattices for quantum computing with alkaline-earth-metal atoms, *Eur. Phys. J. D* 65, 207 (2011)
77. A. J. Daley, Quantum computing and quantum simulation with group-II atoms, *Quant. Inf. Proc.* 10, 865 (2011)
78. G. Pagano, F. Scazza, and M. FossFeig, Fast and scalable quantum information processing with two electron atoms in optical tweezer arrays, *Adv. Quant. Technol.* 2, 1970021 (2019)
79. J. H. M. Jensen, J. J. Sørensen, K. Mølmer, and J. F. Sherson, Time-optimal control of collisional SWAP gates in ultracold atomic systems, *Phys. Rev. A* 100, 052314 (2019)
80. R. Stock, N. S. Babcock, M. G. Raizen, and B. C. Sanders, Entanglement of group-II-like atoms with fast measurement for quantum information processing, *Phys. Rev.* 78, 022301 (2008)
81. M. Saffman and T. G. Walker, Analysis of a quantum logic device based on dipole-dipole interactions of optical-lytrapped Rydberg atoms, *Phys. Rev. A* 72, 022347(2005)
82. M. Saffman, X. L. Zhang, A. T. Gill, L. Isenhower, and T. G. Walker, Rydberg state mediated quantum gates and entanglement of pairs of neutral atoms, *J. Phys.: Conf. Ser.* 264, 012023 (2011)
83. S. G. Porsev, A. Derevianko, and E. N. Fortson, Possibility of an optical clock using the $6^1S_0 \rightarrow 6^3P_0^o$ transition in $^{171,173}\text{Yb}$ atoms held in an optical lattice, *Phys. Rev. A* 69, 021403(R) (2004)
84. B. Budick and J. Snir, Hyperfine structure of the $6s6p^1P_1$ level of the stable ytterbium isotopes, *Phys. Rev.* 178, 18 (1969)
85. R. W. Berends and L. Maleki, Hyperfine structure and isotope shifts of transitions in neutral and singly ionized ytterbium, *J. Opt. Soc. Am. B* 9, 332 (1992)
86. K. Deilamian, J. D. Gillaspay, and D. E. Kelleher, Isotopeshifts and hyperfine splittings of the 3988-nm Yb I line, *J. Opt. Soc. Am. B* 10, 789 (1993)
87. R. Zinkstok, E. J. Van Duijn, S. Witte, and W. Hogervorst, Hyperfine structure and isotope shift of transitions in Yb I using UV and deep-UV cw laser light and the angular distribution of fluorescence radiation, *J. Phys. B* 35, 2693 (2002)
88. P. E. Atkinson, J. S. Schelfhout, and J. J. McFerran, Hyperfine constants and line separations for the $^1S_0 \rightarrow ^3P_1$ intercombination line in neutral ytterbium with sub-Doppler resolution, *Phys. Rev. A* 100, 042505 (2019)
89. A.-M. Mårtensson-Pendrill, D. S. Gough, and P. Hanaford, Isotope shifts and hyperfine structure in the 369.4-nm $6s-6p_{1/2}$ resonance line of singly ionized ytterbium, *Phys. Rev. A* 49, 3351 (1994)
90. K. B. Blagoev and V. A. Komarovskii, Lifetimes of levels of neutral and singly ionized lanthanide atoms, *At. Data Nucl. Data Tables* 56, 1 (1994)
91. M. M. Boyd, T. Zelevinsky, A. D. Ludlow, S. Blatt, T. Zanon-Willette, S. M. Foreman, and J. Ye, Nuclear spin effects in optical lattice clocks, *Phys. Rev. A* 76(2007)
92. B. Budick and J. Snir, Hyperfine-structure anomalies of stable ytterbium isotopes, *Phys. Rev. A* 1, 545 (1970)
93. K. Pandey, A. K. Singh, P. V. Kumar, M. V. Suryanarayana, and V. Natarajan, Isotope shifts and hyperfine structure in the 555.8-nm $^1S_0 \rightarrow ^3P_1$ line of Yb, *Phys. Rev. A* 80, 022518 (2009)
94. H. Lehec, X. Hua, P. Pillet, and P. Cheinet, Isolated core excitation of high-orbital quantum-number Rydberg states of ytterbium, *Phys. Rev. A* 103, 022806 (2021)
95. G. Higgins, W. Li, F. Pokorny, C. Zhang, F. Kress, C. Maier, J. Haag, Q. Bodart, I. Lesanovsky, and M. Hennrich, A single strontium Rydberg ion confined in a Paul trap, *Phys. Rev. X* 7, 021038 (2017)
96. G. Higgins, F. Pokorny, C. Zhang, Q. Bodart, and M. Hennrich, Coherent control of a single trapped Rydberg ion, *Phys. Rev. Lett.* 119, 220501 (2017)
97. C. Zhang, F. Pokorny, W. Li, G. Higgins, A. Pöschl, I. Lesanovsky, and M. Hennrich, Submicrosecond entangling gate between trapped ions via Rydberg interaction, *Nature* 580, 345 (2020)
98. X.-F. Shi, Fast, Accurate, and realizable two-qubit entangling gates by quantum interference in detuned Rabi cycles of Rydberg atoms, *Phys. Rev. Appl.* 11, 044035 (2019)
99. X. L. Zhang, A. T. Gill, L. Isenhower, T. G. Walker, and M. Saffman, Fidelity of a Rydberg-blockade quantum gate from simulated quantum process tomography, *Phys. Rev. A* 85, 042310 (2012)
100. X.-F. Shi, Accurate quantum logic gates by spin echo in Rydberg atoms, *Phys. Rev. Appl.* 10, 034006 (2018)
101. L. H. Pedersen, N. M. Møller, and K. Mølmer, Fidelity of quantum operations, *Phys. Lett. A* 367, 47 (2007)
102. E. J. Robertson, N. Šibalić, R. M. Potvliege, and M. P. A. Jones, ARC 3.0: An expanded Python toolbox for atomic physics, *Comp. Phys. Comm.* 261, 107814 (2021)
103. H. Lehec, A. Zuliani, W. Maineult, E. Luc-Koenig, P. Pillet, P. Cheinet, F. Niyaz, and T. F. Gallagher, Laser and microwave spectroscopy of even-parity Rydberg states of neutral ytterbium and multichannel quantum defect theory analysis, *Phys. Rev. A* 98, 062506 (2018)
104. B. Kaulakys, Consistent analytical approach for the quasi-classical radial dipole matrix elements, *J. Phys. B* 28, 4963 (1995)
105. X.-F. Shi, F. Bariani, and T. A. B. Kennedy, Entanglement of neutral-atom chains by spin-exchange Rydberg interaction, *Phys. Rev. A* 90, 062327 (2014)

106. X.-F. Shi, Transition slow-down by Rydberg interaction of neutral atoms and a fast controlled-NOT quantum gate, *Phys. Rev. Appl.* 14, 054058 (2020)
107. J. S. Ross and K. Murakawa, Nuclear quadrupole moment of Yb¹⁷³, *Phys. Rev.* 128, 1159 (1962)
108. M. Aymar, Multichannel-quantum-defect theory wavefunctions of Ba tested or improved by laser measurements, *J. Opt. Soc. Am. B* 1, 239 (1984)
109. L. Xingye, L. Wanfa, J. Zhankui, and J. Larsson, Test of the multichannel quantum-defect wave function by a Landé-factor (g_J) investigation in the perturbed $6snp\ ^{1,3}P_1$ sequences of Yb I, *Phys. Rev. A* 49, 4443 (1994)
110. T. Ido and H. Katori, Recoil-free spectroscopy of neutral Sr atoms in the Lamb–Dicke regime, *Phys. Rev. Lett.* 91, 053001 (2003)
111. S. Ye, X. Zhang, T. C. Killian, F. B. Dunning, M. Hiller, S. Yoshida, S. Nagele, and J. Burgdörfer, Production of very-high- n strontium Rydberg atoms, *Phys. Rev. A* 88, 043430 (2013)
112. C. Gaul, B. J. DeSalvo, J. A. Aman, F. B. Dunning, T. C. Killian, and T. Pohl, Resonant Rydberg dressing of alkaline-earth atoms via electromagnetically induced transparency, *Phys. Rev. Lett.* 116, 243001 (2016)
113. M. N. Winchester, M. A. Norcia, J. R. K. Cline, and J. K. Thompson, Magnetically Induced optical transparency on a forbidden transition in strontium for cavity-enhanced spectroscopy, *Phys. Rev. Lett.* 118, 263601 (2017)
114. R. Ding, J. D. Whalen, S. K. Kanungo, T. C. Killian, F. B. Dunning, S. Yoshida, and J. Burgdörfer, Spectroscopy of Sr⁸⁷ triplet Rydberg states, *Phys. Rev. A* 98, 042505 (2018)
115. H. G. C. Werij, C. H. Greene, C. E. Theodosiou, and A. Gallagher, Oscillator strengths and radiative branching ratios in atomic Sr, *Phys. Rev. A* 46, 1248 (1992)
116. C. L. Vaillant, M. P. Jones, and R. M. Potvliege, Long-range Rydberg–Rydberg interactions in calcium, strontium and ytterbium, *J. Phys. B: At. Mol. Opt. Phys.* 45, 135004 (2012)
117. C. L. Vaillant, M. P. Jones, and R. M. Potvliege, Multichannel quantum defect theory of strontium bound Rydberg states, *J. Phys. B: At. Mol. Opt. Phys.* 47, 155001 (2014)
118. F. B. Dunning, T. C. Killian, S. Yoshida, and J. Burgdörfer, Recent advances in Rydberg physics using alkaline-earth atoms, *J. Phys. B* 49, 112003 (2016)
119. F. Robicheaux, Calculations of long range interactions for ⁸⁷Sr Rydberg states, *J. Phys. B* 52, 244001 (2019)
120. R. Mukherjee, J. Millen, R. Nath, M. P. Jones, and T. Pohl, Many-body physics with alkaline-earth Rydberg lattices, *J. Phys. B* 44, 184010 (2011)
121. X. Zhang, F. B. Dunning, S. Yoshida, and J. Burgdörfer, Rydberg blockade effects at $n \sim 300$ in strontium, *Phys. Rev. A* 92, 051402(R) (2015)
122. B. J. DeSalvo, J. A. Aman, C. Gaul, T. Pohl, S. Yoshida, J. Burgdörfer, K. R. A. Hazzard, F. B. Dunning, and T. C. Killian, Rydberg–blockade effects in Autler–Townes spectra of ultracold strontium, *Phys. Rev. A* 93, 022709 (2016)
123. S. Yoshida, J. Burgdörfer, X. Zhang, and F. B. Dunning, Rydberg blockade in a hot atomic beam, *Phys. Rev. A* 95, 042705 (2017)
124. J. E. Sansonetti and G. Nave, Wavelengths, transition probabilities, and energy levels for the spectrum of neutral strontium (Sr I), *J. Phys. Chem. Ref. Data* 39, 033103 (2010)
125. R. J. Fonck, F. L. Roesler, D. H. Tracy, K. T. Lu, F. S. Tomkins, and W. R. S. Garton, Atomic diamagnetism and diamagnetically induced configuration mixing in laser-excited barium, *Phys. Rev. Lett.* 39, 1513 (1977)
126. C. Ates, T. Pohl, T. Pattard, and J. M. Rost, Antiblockade in Rydberg excitation of an ultracold lattice gas, *Phys. Rev. Lett.* 98, 023002 (2007)
127. T. Amthor, C. Giese, C. S. Hofmann, and M. Weidemüller, Evidence of antiblockade in an ultracold Rydberg gas, *Phys. Rev. Lett.* 104, 013001 (2010)
128. S.-L. Su, F.-Q. Guo, J.-L. Wu, Z. Jin, X. Q. Shao, and S. Zhang, Rydberg antiblockade regimes: Dynamics and applications, *EPL* 131, 53001 (2020)
129. A. Lurio, M. Mandel, and R. Novick, Second-order hyperfine and Zeeman corrections for an (sl) configuration, *Phys. Rev.* 126, 1758 (1962)
130. D. W. Fang, W. J. Xie, Y. Zhang, X. Hu, and Y. Y. Liu, Radiative lifetimes of Rydberg state of ytterbium, *J. Quant. Spectrosc. Ra.* 69, 469 (2001)
131. J. P. Covey, A. Sipahigil, and M. Saffman, Microwave-to-optical conversion via four-wave mixing in a cold ytterbium ensemble, *Phys. Rev. A* 100, 012307 (2019)
132. D. A. Steck, Quantum and Atom Optics, <http://steck.us/teaching>
133. T. G. Walker and M. Saffman, Consequences of Zeeman-degeneracy for the van der Waals blockade between Rydberg atoms, *Phys. Rev. A* 77, 032723 (2008)
134. T. Zelevinsky, M. M. Boyd, A. D. Ludlow, T. Ido, J. Ye, R. Ciurylo, P. Naidon, and P. S. Julienne, Narrow line photo association in an optical lattice, *Phys. Rev. Lett.* 96, 203201 (2006)
135. J. Millen, G. Lochead, and M. P. A. Jones, Two electron excitation of an interacting cold Rydberg gas, *Phys. Rev. Lett.* 105, 213004 (2010)